Dinuclear Complexes of Uranyl, Neptunyl and Plutonyl: Structures and Oxidation States Revealed by Experiment and Theory

Tian Jian[1], Monica Vasiliu[2], Zachary R. Lee,[2,3] Zhicheng Zhang,[1] David A. Dixon[2,*], John K. Gibson[1,*]

[1] Chemical Sciences Division, Lawrence Berkeley National Laboratory, Berkeley, California, 94720, USA

[2] Department of Chemistry and Biochemistry, University of Alabama, Tuscaloosa, Alabama, 35401, USA

[3] Department of Biology and Chemistry, Morehead State University, Morehead, Kentucky, 40351, USA.

*Corresponding author email: dadixon@ua.edu; jkgibson@lbl.gov

Abstract

Dinuclear perchlorate complexes of uranium, neptunium and plutonium were characterized by reactivity and DFT, with results revealing structures containing pentavalent, hexavalent and heptavalent actinyls, and actinyl-actinyl interactions (AAIs). Electrospray ionization produced native complexes $[(AnO_2)_2(ClO_4)_3]^-$ for An:An = U:U, Np:Np, Pu:Pu and Np:Pu, which are intuitively formulated as actinyl(V) perchlorates. However, DFT identified lower-energy structures $[(AnO_2)(AnO_3)(ClO_4)_2(ClO_3)]^-$ comprising a perchlorate fragmented to ClO_3, actinyl(VI) cation $An^{VI}O_2^{2+}$ and neutral AnO_3. For U:U and Np:Np, and Np in Np:Pu, the coordinated AnO_3 is calculated as actinyl(VI) with an equatorial oxo, $[O_{yl}=An^{VI}=O_{yl}][=O_{eq}]$, whereas for Pu:Pu it is plutonyl(V) oxyl, $[O_{yl}=Pu^{V}=O_{yl}][-O^{\bullet}_{eq}]$. The implied lower stability of Pu^{VI} versus Np^{VI} indicates weaker $Pu=O_{eq}$ versus $Np=O_{eq}$ bonding. Adsorption of O_2 by the U:U complex suggests oxidation of U^{V} to U^{VI}, corroborating the assignment of perchlorate $[(An^{V}O_2)_2(ClO_4)_3]^-$. DFT predicts the O_2-adducts are $[(An^{VI}O_2)(O_2)(An^{VI}O_2)(ClO_4)_3]^-$ with actinyls oxidized from +V to +VI by bridging peroxide, O_2^{2-}. In accord with reactivity, O_2-addition is computed as substantially exothermic for U:U and least favorable for Pu:Pu. Collision induced dissociation of native complexes eliminated ClO_2 to yield $[(AnO_2)(O)_2(AnO_2)(ClO_4)_2]^-$ in which fragmented O atoms bridge as oxyl $O^{-\bullet}$ and oxo O^{2-} to yield uranyl(VI) and plutonyl(VI), or as oxos O^{2-} to yield neptunyl(VII), $[O_{yl}=Np^{VII}=O_{yl}]^{3+}$.

Introduction

In contrast to complexes with only one metal center, dinuclear complexes enable structural and electronic control of properties via interactions between the metal centers.[1] Such interactions in isolated gas-phase complexes are free of perturbations due to coordination in condensed phase. The metals in a dinuclear complex may be the same (homonuclear) or different (heteronuclear), and the interaction between them may be direct or through bridging ligands. Actinyl dioxo cations—pentavalent $An^{V}O_2^{+}$ and hexavalent $An^{VI}O_2^{2+}$ (An = U, Np, Pu)—can exhibit so-called actinyl-actinyl interactions (AAIs; sometimes called cation-cation interactions), in end-on or side-on fashions as shown in Scheme 1.[2] The AAI is between polar actinyl cations, $[^{\delta-}O{=}An^{(2\delta+n)+}{=}O^{\delta-}]^{n+}$ where n = 1 for An^{V} and n = 2 for An^{VI}. Effective charges in uranyl(VI), for example, are +3.2 e on U and -0.6 e on O_{yl}, i.e., $[^{0.6-}O{=}U^{3.2+}{=}O^{0.6-}]^{2+}$.[3-4] Condensed phase AAIs are prevalent for pentavalent actinyls like neptunyl(V),[5-6] whereas less common for dipositive hexavalent actinyls due to greater Coulombic repulsion.[2, 7-9]

Small gas-phase complexes are well-suited for high level ab initio electronic structure computations to provide elucidation that may be relevant to understanding more complicated condensed phase systems. Electronic structure calculations for bare AAI dimers $[(An^{V,VI}O_2^{+,2+})(An^{V,VI}O_2^{+,2+})]$ having various combinations of An^{V} and An^{VI} predicted their inherent instability towards dissociation to the separated actinyl cations.[10] Coordinating ligands can stabilize gas-phase AAIs,[11] as in uranyl dicarboxylate dimers, $[(U^{V}O_2^{+})(^{-}OOC\text{-}[CH_2]_n\text{-}COO^{-})_2(U^{VI}O_2^{2+})]^{-}$ ($n \geq 3$).[12] In contrast to long flexible dicarboxylate linkers that *allow* AAI orientations, short stiff bridging ligands might *impose* AAIs. Perchlorate, ClO_4^{-}, is potentially such an *imposing* ligand, though its coordination efficacy can be limited by low charge density,[13-14] and its high reactivity often precludes practical applications. Nonetheless, perchlorate has been demonstrated to exhibit bidentate coordination,[15] and bridging to support metal-metal interactions, [16-17] such as between the manganese centers in $[Mn_2(ClO_4)_3(H_2O)_{2\text{-}5}]^{+}$.[18]

As for d-block transition metals, insight into f-block chemistry is enhanced by comparing several members of the series, although for most 5f actinides this tack is hindered by radioactivity and scarcity. Actinyl(V) and actinyl(VI) oxidation states are known for U, Np, Pu and Am, with uranyl(VI), neptunyl(V) and plutonyl(V) particularly prevalent under environmental conditions,[19] and americyl less common.[20] The role of AAIs in condensed phase processes such as redox is illustrated by disproportionation of uranyl(V) to U^{4+} and uranyl(VI) mediated by a U^{VI}/U^{V} AAI.[21]

The demonstrated ability of perchlorate to support condensed phase metal-metal interactions,[16-17] suggests it as a candidate to similarly facilitate AAIs in the gas phase. To pursue this prospect, dinuclear actinyl complexes, $[(AnO_2)_2(ClO_4)_3]^{-}$, were prepared by electrospray ionization (ESI) of perchlorate solutions containing uranyl, neptunyl and/or plutonyl. These native complexes were studied for actinide pairs An:An = U:U, Np:Np, Pu:Pu and Np:Pu. Only for the U:U complex was O_2 adsorbed in an ion-molecule reaction, presumably resulting in oxidation of uranyl(V) to uranyl(VI) by peroxide formation, as has previously been reported for complexes such as $[(U^{VI}O_2)_2(O_2)(L)_2]^{2+}$ (L is a functionalized diacetamide).[22] Because neptunyl(V) and plutonyl(V) are more resistant to such oxidation,[23] the Np:Np, Pu:Pu and Np:Pu native complexes

do not similarly adsorb O_2. Density functional theory (DFT) results are in accord with this intuitive assessment of the observed reactivity and furthermore indicate that the native complexes feature actinyl(V) AAIs supported by perchlorate, $[(An^{V}O_2)\cdots(An^{V}O_2)(ClO_4)_3]^-$, with addition of O_2 in a bridging mode disrupting the AAI. Evaluation of collision induced dissociation (CID) of the native complexes suggests it occurs by perchlorate fragmentation with the liberated O atoms oxidizing the actinyl(V), respectively to uranyl(VI), plutonyl(VI) and neptunyl(VII). Experimental results are also presented for nitrate and chloride complexes.

Experimental and Computational Methods

Caution - Isotopes ^{238}U, ^{237}Np and ^{242}Pu are radioactive and must be handled using appropriate safeguards.

Experiments were performed using an Agilent 6340 quadrupole ion trap mass spectrometer (QIT-MS) with ionization by an ESI source located inside a radiological containment glove box as described previously.[24] Native complexes, $[(AnO_2)_2X_3]^-$ (An = ^{238}U, ^{237}Np, ^{242}Pu; X = ClO_4, NO_3, Cl), were produced by ESI of ethanol:water (1:1 by volume) solutions containing 0.2-0.5 mM of one or two actinyl salts, AnO_2X_3. The target gas-phase complex was isolated in the QIT and subjected to collision induced dissociation (CID), whereby resonant excitation results in multiple energetic collisions with helium that induce dissociation; products are identified by mass-selective ejection. The CID energy is not quantified but increases in parallel with the instrumental setting. Ion-molecule reactions (IMRs) of thermalized trapped ions with background gases were studied by retaining a mass-selected ion for a designated reaction time with no applied excitation voltage. The reaction time was usually 10 s, but was reduced to 0.8 s in cases of very low abundance of the reactant ion. The following instrumental parameters were employed: solution flow rate, 60-90 μL/min; nebulizer gas pressure, 15 psi; capillary voltage, 3500 V; end plate voltage offset, -500 V; dry gas flow rate, 5 L/min; dry gas temperature, 325 °C; capillary exit, -166.7 V; skimmer, -46.2 V; octopole 1 and 2 dc, -10.4 and 0.00 V; octopole RF amplitude, 270.8 V_{pp}; lens 1 and 2, 9.0 and 100.0 V; trap drive, 83.2. High-purity nitrogen gas for nebulization and drying in the ion transfer capillary was boil-off from a liquid nitrogen Dewar. The QIT helium buffer gas pressure was $\sim 10^{-4}$ Torr; background H_2O and O_2 pressures were estimated as $\sim 10^{-6}$ Torr.[23]

The DFT calculations were performed with the B3LYP exchange-correlation functional[25-26] with the aug-cc-pVDZ for O,[27] the aug-cc-pVD(+d)Z for Cl,[28] and the Stuttgart basis sets and associated small core effective core potentials (ECP) for the actinides.[29-31] Geometries were optimized and second derivatives were calculated to ensure that the structures were minima and to provide vibrational frequencies for the thermodynamic calculations. The values of S^2 are given in the SI. High spin states exhibit little spin contamination but lower spin states for the same structure can exhibit significant spin contamination as would be expected from spin polarization and the mixing in of higher spin states. All calculations were performed with Gaussian16.[32] The default settings in Gaussian16 were used for the calculations.

Results and Discussion

Native Complexes - Preparation and Structure Prediction

ESI of solutions of uranyl, neptunyl and/or plutonyl with perchlorate, nitrate or chloride produced the so-called native complexes. The following dominant oxidation states are assigned by assuming cations An^{3+}, An^{4+}, $An^{V}O_2^{+}$ or $An^{VI}O_2^{2+}$ coordinated by anions Cl^-, ClO_4^- or NO_3^-: U^{VI} Np^{V}, Pu^{III}, Pu^{IV}, Pu^{V} and Pu^{VI}. Such coexistence of four plutonium oxidation states reflects its VI/V, V/IV and IV/III reduction potentials in the narrow range of 0.94-1.06 V.[33] The focus is on native dinuclear complexes $[(AnO_2)_2(X)_3]^-$ having An = U, Np or Pu and X = ClO_4, NO_3 or Cl; the assumption that these comprise actinyl(V) moieties, $An^{V}O_2^{+}$, is assessed below. Experiments were performed for the following nine combinations of anion X with actinide pair An:An: ClO_4^- with U:U, Np:Np, Pu:Pu and Np:Pu; NO_3^- with U:U and Np:Np; Cl^- with U:U, Np:Np and U:Np. The "soft" nature of ESI is often invoked to infer solution speciation, though actual relationships between solution and gas are often convoluted.[34] Solution speciation is not inferred here, but a more conservative assumption is invoked (and later corroborated) that ClO_4 and NO_3 ligands remain intact during ESI.[35-36]

The electronic structure calculations focused on perchlorate complexes $[(AnO_2)_2(ClO_4)_3]^-$ for actinide pairs U:U, Np:Np, Pu:Pu and Np:Pu. To assess the assumption that the perchlorates remain intact, calculations were also performed for structures with fragmented perchlorate. In structures with a ClO_3^- or ClO_2^- fragment the liberated O atom(s) coordinate and oxidize the actinyl, from +V to +VI or +VII. Structures **A**, **B**, **C** and **D** were optimized for native complexes $[(AnO_2)_2(ClO_4)_3]^-$ and are shown in Figure 1, with energies and nominal oxidation states in Table 1. Bonds unambiguously covalent, like perchlorate Cl-O_L (O_L = ligand oxygen) and actinyl An=O_{yl}, are depicted as solid connections in Figure 1, whereas dative bonds like An···O_L are dashed. The distinction between covalent and dative bonding is sometimes blurred, such as for AAI bond ***c*** in structure **A** discussed below.

Structures **A** and **B** incorporate a perchlorate fragmented to $[ClO_3^- + O]$ or $[ClO_2^- + 2O]$, respectively, whereas all ligands are intact in **C** and **D**. Note that the chlorine oxide fragments remain negatively charged. The O transferred to the actinide oxide may have oxidation states of -1 or -2 depending on which complex, oxyl or oxo, is formed with corresponding oxidation state changes in the resultant actinide oxides. After first summarizing key characteristics of **B** and **C**, the emphasis is on **A**, which is predicted to be the lowest energy structure for U:U, Np:Np and Np:Pu, and **D**, which is lowest energy for Pu:Pu (Table 1). A variety of spin states for the complexes were examined.

Structure **C** has two actinyl(V) moieties, AnO_2^{+}, coordinated by bridging and terminal perchlorates with no actinyl-actinyl interactions. Parameters for **C** given in Figure 1 for the U:U complex indicate nearly linear actinyls with characteristic short An=O_{yl} bonds. Although both **C** and **D** have intact perchlorates and oxidation state An^{V}, **D**, is predicted to be lower in energy by ~28 kcal/mol for U:U, ~11 kcal/mol for Np:Np, ~9 kcal/mol for Pu:Pu and ~24 kcal/mol for

Np:Pu. Structure **C** just has the high spin coupling of two AnO_2^+ with the An in the +V oxidation state.

Structure **B** for U:U is composed of two UO_3^+ with a spin on each O_{eq}^- and U in the +VI oxidation state. For Np:Np, this results in a lowest energy singlet state for isomer **B** with two NpO_3^+ each with Np in the +VII state. For Pu:Pu, the structure is made up of two PuO_3^+ with the Pu in the +VI oxidation state with 2 unpaired electrons on each Pu and two equatorial O^- atoms each with a spin. The three states that arise depend on the coupling of the oxygen spin (α or β) with the approximately two α spins on each Pu +VI. The spin polarized low spin coupled states are slightly lower in energy than the high spin coupled state.

In structure **B**, a perchlorate is fragmented to ClO_2^- with the two liberated O atoms transforming the actinyls AnO_2^+ to AnO_3^+, which are coordinated by a bridging ClO_2^- and two terminal ClO_4^-. The AnO_3^+ moieties in **B** can be considered actinyls, $[O_{yl}=An=O_{yl}]$, coordinated by an equatorial oxygen (O_{eq}). The effective charges and oxidation states are established by this O_{eq} as $An^{VI}O_2^{2+}$ in case of oxyl $An\text{-}O_{eq}^{\bullet}$, or as $An^{VII}O_2^{3+}$ for oxo $An=O_{eq}$. For the U:U, Np:Np and Pu:Pu complexes the lowest energy isomer is oxyl $An^{VI}O_2(\text{-}O_{eq}^{\bullet})$, whereas for Np:Pu it is a combination of oxyl $Pu^{VI}O_2(\text{-}O_{eq}^{\bullet})$ and oxo $Np^{VII}O_2(=O_{eq})$. Coexistence of Pu^{VI} and Np^{VII} in the latter reveals relatively facile oxidation to heptavalent Np, as is known to also occur in the condensed phase.[33, 37-40] The An-O_{eq} distance in **B** for U:U (2.10 Å) is somewhat longer than for Np:Np (1.84 Å) but similar to Pu:Pu (2.05 Å). For Np^{VII}:$Pu^{V/VI}$, Np^{VII}-O_{eq} = 1.84 Å and $Pu^{V/VI}$-O_{eq} = 2.10 Å; for Np^{VI}:Pu^{VI}, Np^{VI}-O_{eq} = 2.08 Å and Pu^{VI}-O_{eq} = 2.12 Å; for Np^{VII}:Pu^{VI}, Np^{VII}-O_{eq} = 1.84 Å and Pu^{VI}-O_{eq} = 2.10 Å. The spin on O_{eq} in the PuO_3 fragment in Np^{VII}:Pu^{VI} is 0.92 and there is no spin on the NpO_3 O_{eq} consistent with a charge of -2 on this oxygen. Similarly, Np^{VII}:$Pu^{V/VI}$ has -1.12 spin on the O_{eq} in the PuO_3 fragment and there is no spin on the NpO_3 O_{eq}, again consistent with a charge of -2 on this oxygen. For Np^{VI}:Pu^{VI}, the NpO_3 O_{eq} has 0.93 excess α electrons and the PuO_3 O_{eq} has 0.97 excess α electrons.

For structure **A**, starting from two AnO_2^+, U:U has up to two unpaired spins, Np:Np has up to four unpaired spins, Pu:Pu has up to six unpaired spins, and Np:Pu has up to five unpaired spins. The Mulliken spin populations (Supporting Information) are important in assigning the oxidation states of the actinides. For structure **A**, for U:U, if the structure $U_2O_5^{2+}$ is a singlet, then it is composed of a UO_2^{2+} and a UO_3, both of which are singlets as found. For Np:Np, we would expect a triplet for NpO_2^{2+} and a NpO_3 and this is the lowest energy spin state for **A**. Following this model, we would expect a quintet to be the lowest energy structure for Pu:Pu for **A** but although the quintet is predicted to be of low energy, the lowest energy form is likely to be the septet which is a PuO_2^{2+} with 2 unpaired spins, and a PuO_3 with the Pu in a +V oxidation with 3 unpaired spins, and an O with one unpaired spin. The quintet state just has the spin on O flipped so it is highly spin polarized. For Np:Pu, the spins show that the lowest energy sextet is PuO_2^+ and an NpO_3^+ with Np in the +VI oxidation state and a spin on the O^-. Essentially identical in energy is a structure with a PuO_2^{2+} with 2 unpaired spins for a Pu +VI, and a NpO_3 with Np in the +VI oxidation state with one unpaired spin on the Np.

The bond distances and angles labelled on structure **A** in Figure 1 are given in Table 2. The core of **A** consists of cation AnO_2^{2+} and neutral AnO_3—forming an $An_2O_5^{2+}$ cluster—coordinated by ClO_4^- and ClO_3^- with An···O_L distances in the range 2.37-2.54 Å. For all four An:An pairs the AnO_2^{2+} moiety is actinyl(VI) with nearly linear O_{yl}=An=O_{yl} (***α*** = 178°-179°) and short An=O_{yl} distances ***a*** and ***a′*** (1.72-1.82 Å). For U:U, Np:Np and Np:Pu, the AnO_3 moiety has three oxo bonds—two short distances ***b′*** and ***b″*** (1.79-1.84 Å) and slightly longer ***b*** (1.95-2.02 Å)—which render it to have a bent actinyl(VI) (**β** = 162°-166°). Notably, the equatorial An=O_{eq} bond ***b″*** is shorter than An=O_{yl} bond ***b***. Elongation of ***b*** is accompanied by participation of that O_{yl} in an AAI with bond distance ***c*** (2.19-2.24 Å) which is only slightly longer than a typical An-O single bond (e.g., ***b″*** = 2.15 Å for Pu:Pu). For the Np:Pu complex, structure **A** contains $Pu^{VI}O_2^{2+}$ and $Np^{VI}O_3$, whereas for Pu:Pu it is $Pu^{VI}O_2^{2+}$ and $Pu^{V}O_3$ where the latter is linear plutonyl(V) coordinated by oxyl Pu-$O_{eq}^{\bullet}$ (distance ***b″*** = 2.15 Å). The nature of these AnO_3 moieties is elaborated below. In all cases, the $An_2O_5^{2+}$ core of **A** features an AAI with the bond distances ***c*** and ***c′*** longer for the Pu^{V}:Pu^{VI} complex versus the three An^{VI}:An^{VI} complexes (Table 2). The weaker plutonyl(V/VI) AAI is likely due to lower actinide charge—(2δ+n)+ in $[^{\delta-}O=An^{(2\delta+n)+}=O^{\delta-}]^{n+}$—for actinyl(V) (n=1) versus actinyl(VI) (n=2).

Structure **D** is predicted to be more stable energetically than **A** for Pu:Pu, by 15 kcal/mol, whereas **A** is more stable for U:U and Np:Np by 53 and 21 kcal/mol respectively, and the two structural isomers are similar in energy to within ~1 kcal/mol for Np:Pu. Nonetheless, in all four cases **D** is likely the actual structure in the experiment as it is the lowest energy containing all perchlorates intact, as assumed above for ESI preparation conditions and substantiated below. Structure **D**, like **C**, has two actinyl(V) coordinated by perchlorates. In **C** a bridging perchlorate intervenes between the actinyls, whereas in **D** two bidentate perchlorates girdle the actinyls and support—or, as described above, *impose*—a side-on AAI (Figure 1). The actinyl(V) in **D** have short An=O_{yl} bonds (**a**, **a′**, **b** and **b′**, 1.76 - 1.94 Å) with minor deviations from linear O_{yl}=An=O_{yl} (**α, β** = 173°-179°). The AAI distances ***c′*** (2.26 - 2.36 Å) are similar to condensed phase AAIs and shorter than typical An···O_L distances.[41] The AAI in **D** is asymmetric, with ***c*** (2.40-2.56 Å) slightly longer than ***c′*** (2.26-2.36 Å). The An=O_{yl} bond for the O_{yl} participating in the AAI is elongated, with ***a′*** longer than ***a*** by ~0.1 Å. Distances ***c*** and ***c′*** exhibit the opposite trend expected from the actinide contraction, with the shortest/strongest AAI bonds for U:U and the longest/weakest for Pu:Pu. This suggests greater An=O_{yl} bond ionicity and more positive charge on the actinide center in uranyl(V) versus other actinyl(V), as is known to be the case in solution.[42] Structure **D** is just the high spin coupling of two AnO_2^+ with the An in the +V oxidation state.

Coordinated AnO_3 - Oxidation States and Bonding

The actinide trioxides embedded in structure **A** can be compared with bare AnO_3 molecules, which have been reported for An = U[43] and Pu.[44] The UO_3 molecule has been characterized as having a T-shaped structure consisting of a nearly linear uranyl(VI) coordinated by an equatorial oxo, [O_{yl}=U^{VI}=O_{yl}][=O_{eq}], a motif comparable to the UO_3 moiety in **A**.[45-47] The trioxide bond dissociation energies for the equatorial O, D[OU_2-O] = 139 kcal/mol versus

D[OPu_2-O] = 93 kcal/mol,[47] indicate diminished An=O_{eq} bonding for PuO_3 versus UO_3, which parallels dioxide AnO_2 bond energies (D[OAn-O] = 179 for U; 151 for Np; 143 kcal/mol for Pu).[48] Kovács reviewed computational studies of UO_3, NpO_3 and PuO_3, which are computed to be actinyl(VI) coordinated by equatorial oxo, in accord with experimental results for UO_3.[49] For trioxides of transuranium actinides, actinyl(VI) structures are predicted to decrease in stability relative to lower oxidation states, with AmO_3 comprising oxyl-coordinated americyl(V).[50] After americium, the lowest energy CmO_3 isomer is not oxygen-coordinated curyl, (O=Cm=O)(O), but rather trivalent Cm mono-oxo superoxide, $O=Cm^{III}(\eta^2\text{-}O_2)$.[51]

The same oxidation state characteristics reported for bare AnO_3 appear in isomer **A** comprising $U^{VI}O_3$, $Np^{VI}O_3$ and $Pu^{V}O_3$ in the U:U, Np:Np and Pu:Pu complexes. Referring to atom labels for **A** in Figure 1, for Np:Pu the An(*1*) site is plutonyl(VI), $Pu^{VI}O_2^{2+}$, and An(*2*) is $Np^{VI}O_3$ with oxo Np=O_{eq}. For Pu:Pu, the An(*1*) site is also plutonyl(VI), but An(*2*) is $Pu^{V}O_3$ with oxyl Pu-$O_{eq}^{-\bullet}$. Since formation of $Np^{VI}O_3$ versus $Pu^{V}O_3$ is a result of oxo in $[O_{yl}=Np^{VI}=O_{yl}][=O_{eq}]$ versus oxyl in $[O_{yl}=Pu^{V}=O_{yl}][-O^{\bullet}_{eq}]$, the lower stability of Pu^{VI} indicates weaker oxo bonding, $Pu^{VI}=O_{eq}$. As for other actinide-ligand multiple bonds such as actinyl An=O_{yl}, equatorial oxo bonds are expected to be substantially covalent.[52] Control of actinyl oxidation state by equatorial oxo versus oxyl bonding contrasts with solution redox properties, which are governed by formation and solvation of cations $An^{V}O_2^{+}$ or $An^{VI}O_2^{2+}$. The apparent diminishment in efficacy of An=O_{eq} bonding that results in relative destabilization of the hexavalent state from U to Pu in the complexes parallels decreasing bond energies for the corresponding bare actinyls.[48]

Comparative stabilities of oxidation states An^{VI} in **A** versus An^{V} in **D** are revealed by the energy difference $\Delta E_{\mathbf{DA}} \equiv E[\mathbf{D}] - E[\mathbf{A}]$ (Table 1, kcal/mol): 53.2 for U:U; 20.8 for Np:Np; 1.0 for Np:Pu; and -15.3 for Pu:Pu. These differences show oxidation from +V to +VI is most favorable for U and least so for Pu. For comparison, solution reduction potentials, $E°$(VI/V), follow the order: U (0.16 V, easiest to oxidize to +VI) << Pu (0.97 V) < Np (1.24 V) < Am (1.59 V).[33] Higher stability of U^{VI} versus both Np^{VI} and Pu^{VI} arises in both solution and the gas-phase complexes. However, the result that $\Delta E_{\mathbf{DA}}$ is ~36 kcal/mol higher for Np:Np versus Pu:Pu indicates Np^{VI} as substantially more stable than Pu^{VI} in the complexes, this in contrast to the reverse relationship in solution. This comparison of oxidation states is in accord with the above assessment of AnO_3 moieties in **A**, with both considerations indicating diminished equatorial oxo bonding as the root of reduced stability of oxygen-coordinated plutonyl(VI) in complexes, as compared with bare ion $Pu^{VI}O_2^{2+}$ in solution.

Reactions with O_2 and H_2O

As discussed above, the calculations for the native perchlorates predict that **A** is the lowest energy isomer for U:U and Np:Np, **A** and **D** are similar in energy for Np:Pu, and **D** is the lowest energy isomer for Pu:Pu. However, the actual structure in the ESI experiments in all four cases is hypothesized to be **D** with all perchlorates intact. Comparison of observed and predicted ion-molecule reactions provide a basis to assess this hypothesis. Under near-thermal conditions as employed here, energy conservation requires that an observed bimolecular reaction be exothermic

(or thermoneutral). Results for reactions of the nine native perchlorate, chloride, and nitrate complexes with background O_2 and H_2O are shown in Figures 2, 3, and S4, and summarized in Table 3. Addition of H_2O was observed for the three U:U complexes, the U:Np chloride, and the Np:Np perchlorate. Water-addition to a metal-oxo complex such as an actinyl, and more generically an $[L_n]M{=}O$ moiety, can be categorized using the surface chemistry concepts of *chemisorption* and *physisorption*.[53-54] Water activation in chemisorption produces hydroxide $[L_n]M(OH)_2$, whereas physisorbed water is datively bound in a hydrate, $([L_n]M{=}O){\bullet}(H_2O)$. As the oxidation state is invariant for both types of water adsorption, such reactivity may not readily illuminate the nature of the complexes.

In contrast to adsorption of water, O_2 adsorption by a complex typically results in oxidation of the metal center and may thus better reveal the nature of the reactant complex.[55] The experimental results here for O_2 addition (Table 3) indicate reactivity for the four complexes containing at least one U center; in contrast, complexes containing only actinides Np and/or Pu were practically inert. The gas-phase basicity of H_2O (158 kcal/mol[56]) is sufficient to support hydration at room temperature, whereas the basicity of O_2 (95 kcal/mol[56]) is so low that cryogenic conditions are typically required for physisorption.[57] However, chemisorption of O_2 may produce superoxide O_2^- or peroxide O_2^{2-}, or dissociate to yield two oxyl O^- and/or oxo O^{2-}. For example, O_2 chemisorption by a divalent osmium complex results in four-electron reduction of O_2 to $2(O^{2-})$ concomitant with oxidation of Os^{II} to Os^{VI}.[58] Dissociative chemisorption of O_2 by transition metal ions[59-60] may be facilitated by secondary coordination, such as for hydrated Cr^+.[61] Chemisorption of O_2 by bare uranyl(V), $U^VO_2^+$, yields uranyl(VI) superoxide, η^2-O_2^- $[U^{VI}O_2(\eta^2\text{-}O_2)]^+$, whereas a second O_2 is physisorbed to produce $[U^{VI}O_2(\eta^2\text{-}O_2^-)(\eta^1\text{-}O_2)]^+$.[57] Other examples of uranyl(V) reactivity include O_2 addition to $[(U^VO_2)Cl_2]^-$ and $[(U^VO_2)(H_2O)_3]^+$ to form the respective superoxides, $[(U^{VI}O_2)(O_2)Cl_2]^-$ and $[(U^{VI}O_2)(O_2)(H_2O)_3]^+$.[23, 62-63] In contrast to uranyl(V), the analogous neptunyl(V) and plutonyl(V) complexes do not chemisorb O_2,[23] which reflects less facile oxidation of Np and Pu from +V to +VI.[33]

The result here that O_2 adds to the native $[(AnO_2)_2X_3]^-$ complexes only if there is at least one uranium center suggests that they are actinyl(V) with oxidation accessible for U^V but not Np^V or Pu^V. For chlorides, the notion of ligand fragmentation is irrelevant and assignment as actinyl(V) moieties in $[(An^VO_2)_2Cl_3]^-$ is nearly unambiguous. Addition of O_2 to $[(U^VO_2)_2Cl_3]^-$ and $[(U^VO_2)(Np^VO_2)Cl_3]^-$ is then ascribed to formation of peroxide $[(U^{VI}O_2)(O_2)(U^{VI}O_2)Cl_3]^-$ and superoxide $[(U^{VI}O_2)(O_2)(Np^VO_2)Cl_3]^-$. The homonuclear neptunyl(V) complex, $[(Np^VO_2)_2Cl_3]^-$, is resistant to oxidative addition of O_2. For the native perchlorates and nitrates, observation of O_2-addition only for the U:U complexes is attributed to availability of U^V for oxidation, which excludes structures **A** and **B** and corroborates the assumption that **D** is the structure prepared by ESI.

The above empirical assessment of O_2-addition was complemented by electronic structure calculations. Formulation of the O_2-addition products is $[(AnO_2)_2(O)_2(ClO_4)_3]^-$, rather than $[(AnO_2)_2(O_2)(ClO_4)_3]^-$, to recognize that added oxygen may be as bound O_2 or dissociated to two O. Adduct structures **E**, **F** and **G** are shown in Figure 4, with relative energies in Table 4. All three

isomers have intact perchlorates and oxidation states An^{VI}, in accord with the inference above that addition of O_2 is to native structure **D** and proceeds by oxidation of actinyl(V) to actinyl(VI). The main difference between the three adduct isomers is the disposition of the O_2: **E** has dimer $An_2O_6^{2+}$; **F** has two AnO_3^+; and **G**, the lowest energy structure, has two $An^{VI}O_2^{2+}$ bridged by peroxide O_2^{2-}. Similar to native isomer **D** in which perchlorates bridge in a manner that facilitates an AAI, in **G** a perchlorate links the actinyls in a side-on mode that accommodates the bridging peroxide. Transformation of **D** to **G** corresponds to insertion of O_2 between the actinyls, with disruption of the AAI and rearrangement of a perchlorate from bridging to terminal. The nature of this transformation is sufficiently straightforward that its kinetics are likely governed by the net reaction energy.

Both structures **E** and **F** are higher in energy than **G**. Structure **F** has two AnO_3^+ moieties. For U:U, this yield a triplet with a spin on each O^-. For Np:Np, the most stable structure is a singlet with Np in the +VII oxidation state. For Pu:Pu, the spin is in the +VI oxidation state as for U:U so there is a spin on each O^- as well as the two spins on each Pu. These can be coupled in different ways and there is substantial spin polarization in the quintet and triplet states which affects the energy ordering. For Np:Pu, the Np^{VII}/Pu^{VI} quartet with the O^- group on the Pu is of comparable energy to the Np^{VI}/Pu^{VI} sextet with two O^- groups each with a spin.

The high energy **E** structures are complicated with significant spin polarization in a number of structures. There is clearly an O_2^- bonded side-on to one actinide. For U:U, the triplet is composed of a UO_3:UO^{+3}:O_2^- complex. For Np:Np, the septet is NpO_3^+:NpO^{+2}:O_2^- but the NpO_3^+ has a spin on Np and one on the O^- so the Np oxidation state is +VI, not +VII that might have been expected. The case is more complicated for Pu:Pu but the nonet can be approximately described as PuO_3:PuO^{+3}:O_2^- with the Pu in the PuO_3 in the +V state with an O^- with a spin and the PuO_3^+ having the Pu in the +V oxidation state with 3 unpaired electrons. For the Np:Pu octet, the structure is best described as NpO_3^+:PuO^{+2}:O_2^- where the NpO_3^+ has a spin on Np and one on the O^- so the Np is +VI and the PuO^{+2} has Pu in the +IV oxidation state with 4 unpaired spins. Note that there is spin polarization to the O atoms in all cases.

Selected bond distances and angles given for structures **E** and **F** in Figure 4 for the U:U complex; for lowest energy structure **G** the parameters labelled in Figure 4 are given in Table 5 for all four An:An complexes. Bond orders and oxidation states are inferred from An-O and O-O distances. Short An-O bonds (~1.7-1.8 Å; e.g. ***a*** and ***b*** in **G**) are assigned as An=O oxo, whereas longer bonds (~2.1-2.2 Å; e.g. ***b″*** in **A** for Pu:Pu) are An-$O^\bullet$ oxyl with similar distances to hydroxide single bonds, An-OH.[64-65] The O-O distance in free O_2, 1.21 Å, increases to ~1.2-1.3 Å in superoxide O_2^-, and to ~1.4-1.5 Å in peroxide O_2^{2-}.[66] The bonds in the $U_2O_6^{2+}$ moiety in **E** are assigned as follows (An*1* and An*2* are in this case U*1* and U*2*): U*1* has two U=O oxo (1.81, 1.83 Å) and one U-O single bond (2.08 Å); U*2* has one U=O oxo (1.86 Å) and three U-O single bonds (2.06, 2.07, 2.09 Å), two of which are to a terminal peroxo (η^2-O_2 with O-O distance 1.43 Å). As the net charge on the U_2O_6 cluster in **E** is 2+, the oxidation state is +VI for both U*1* and U*2*. Structure **F** has two $U^{VI}O_3^+$ with short U=O_{yl} oxos (1.77 Å) and longer U-$O^\bullet$ oxyl (2.09 Å).

Geometrical parameters of isomers **E** and **F** for the Np:Np and Pu:Pu complexes are similar to those given in Figure 4 for U:U.

Structure **G** for U:U has two UO_2^{2+} with a 'bridging' peroxide, μ-η^2:η^2-O_2^{2-}, giving an overall singlet. Structure **G** for Np:Np follows the same pattern with a spin on each Np +VI giving a triplet. There is modest spin polarization to all of the oxygens (excess 0.2 α spin on each Np). Pu:Pu has two spins per Pu +VI giving a quintet with a larger amount of spin polarization on the Pu (excess ~ 0.5 α spin on each Pu.) For Np:Pu, we obtain a quartet with one spin on the Np and two spins on the Pu as expected with the same types of spin polarization on each actinide as in the homo-dimers. These are the most stable structures in all cases.

Structure **G** is the lowest energy O_2-adduct, with similar bond distances and angles for all four An:An pairs (Table 5). The added O_2 with O-O distances 1.42-1.45 Å is a peroxide that bridges nearly linear actinyl(VI) moieties. Energies for O_2 addition to the four native structures to produce **G** are in Table 6. For U:U, conversion of **A** to **G** is endothermic by +18.8 kcal/mol, whereas **D** to **G** is exothermic by -34.4 kcal/mol. As the observed addition of O_2 to $[(UO_2)_2(ClO_4)_3]^-$ must be exothermic (or thermoneutral), the computed energies corroborate that the structure of the native complex in the experiment is not the calculated lowest energy **A**, but rather **D** with intact perchlorates. For the other complexes, transformation of presumed structure **D** to **G** is computed as substantially endothermic for Pu:Pu and Np:Pu (19.8 and 12.7 kcal/mol), whereas slightly exothermic for Np:Np (-3.1 kcal/mol). Although exothermic O_2-addition to the Np:Np complex is thus predicted to be (barely) thermodynamically allowed, its non-occurrence may reflect small kinetic barriers above the reactant asymptote energy as well as the accuracy of the DFT calculations.

The prediction that transformation of actinyl(V) in **D** to actinyl(VI) in **G** is substantially exothermic only for U:U parallels more facile solution oxidation for U^V versus Np^V and Pu^V.[33] However, the prediction that oxidation of An^V in **D** to An^{VI} **G** is more favorable for Np versus Pu contrasts with solution oxidation. As remarked above regarding actinide bonding to oxygen ligands in the native complexes, this disparity suggests that actinyl(VI)-peroxide bonding in **G** is more effective for Np than Pu.

Collision Induced Dissociation

The native complexes—assigned above as $[(An^VO_2)_2X_3]^-$ structure **D**—were subjected to CID using a fixed instrumental energy setting of 0.40. CID spectra for the perchlorates are in Figure 5, other CID spectra are in SI, and all CID results are summarized in Table 7. A common pathway was fission reaction (**i**) in which dinuclear $[(An^VO_2)_2X_3]^-$ separates into the detected anion $[(An^VO_2)X_2]^-$, and by inference the neutral $[(An^VO_2)X]$ that cannot be directly detected by mass spectrometry. For the chloride complexes U:U, Np:Np and U:Np, pathway (**i**) was observed (for U:U water addition yielded also minor $[(U^VO_2)_2Cl_3(H_2O)]^-$, Fig. S3). Fission of $[(U^VO_2)(Np^VO_2)Cl_3]^-$ via reaction (**i**) to preferentially $[(U^VO_2)Cl_2]^-$ over $[(Np^VO_2)Cl_2]^-$ suggests stronger chloride binding to uranyl versus neptunyl, in accord with higher uranium charge as inferred above from shorter uranyl(V) AAI distances in complex **D**.

(**i**) ***fission to mononuclear complexes:*** $[(An^{V}O_2)_2X_3]^- \rightarrow [(An^{V}O_2)X_2]^- + [(An^{V}O_2)X]$

In contrast to ESI, CID is inherently energetic and can thus fragment ligands like perchlorate and nitrate, with the released O atoms available to bond to the metal center.[36] For pathway (**i**) in which the compositions do not directly reveal ligand fragmentation the products are presumed to be $[(An^{V}O_2)X_2]^-$ and $[(An^{V}O_2)X]$ in which actinyl(V) are coordinated by intact perchlorates or nitrates. For the nitrates, ligand fragmentation pathways (**iii**), (**iv**) and (**v**) in Table 7 were also observed (CID spectra in Figure S2). Fission pathway (**i**) dominated for the Np:Np nitrate, whereas prevalence of ligand fragmentation for U:U suggests that it involves oxidation of U^{V} to U^{VI}. Pathway (**iii**), for example, produces $[(UO_2)_2(O)_2(NO_3)]^-$, which is presumed to comprise two uranium(VI) trioxide moieties, $[(U^{VI}O_3)(NO_3)(U^{VI}O_3)]^-$.

For perchlorate complexes $[(An^{V}O_2)_2(ClO_4)_3]^-$ the two observed CID pathways are identified in Figure 5 and Table 7: (**i**) (given above, with X = ClO_4) fission to $[(An^{V}O_2)(ClO_4)_2]^-$ + $[(An^{V}O_2)(ClO_4)]$; and (**ii**) (given below) perchlorate ligand fragmentation to $[(AnO_2)_2(O)_2(ClO_4)_2]^-$ + ClO_2.

(**ii**) ***perchlorate fragmentation:*** $[(An^{V}O_2)_2(ClO_4)_3]^- \rightarrow [(AnO_2)_2(O)_2(ClO_4)_2]^- + ClO_2$

For the Np:Np, Pu:Pu and Np:Pu complexes, both pathways (**i**) and (**ii**) were significant, whereas for U:U only pathway (**ii**) was observed. Pathway (**i**) is presumed to retain the An^{V} oxidation state. The particular dominance of (**ii**) for the U:U complex suggests a different model.

In the computational electronic structure assessment of perchlorate pathway (**i**) the anion and neutral products are assumed to be actinyl(V) coordinated by perchlorates, $[(An^{V}O_2)(ClO_4)_2]^-$ and $[(An^{V}O_2)(ClO_4)]$. Computed structure **H** for the product $[(AnO_2)_2(O)_2(ClO_4)_2]^-$ of pathway (**ii**), shown in Figure 6 with relative energies in Table 8, has terminal ClO_4^- coordinating cluster $An_2O_6^+$. Before we discuss structures **H** associated with pathway (**ii**), we consider bare An_2O_6 and $An_2O_6^+$. The U:U neutral dimer U_2O_6 is well established as two UO_2^{2+} linked by two bridging O^{2-}. For Np_2O_6, the preferred structure is a C_{2v} triplet with a closed shell NpO_3^+ fragment in the +VII oxidation state and a NpO_3^- with the Np in the +V oxidation state. The Pu_2O_6 neutral dimer has a complicated structure due to significant spin polarization but is best described as two Pu +VI sites in a distorted U_2O_6 type structure with two spins per Pu. For $NpPuO_6$, the structure is best described as a NpO_3^+ bonded to PuO_3^- with Pu in the +V oxidation state, representing a structure like that of Np_2O_6. For Np:Pu, the lowest energy structure is the triplet with a Np +VII and a Pu +VI with two spins on the Pu.

The removal of the electron from neutral An_2O_6 to generate the $An_2O_6^+$ cations can come from different sites. For U:U, the electron is removed from the O as there are no electrons that can be removed from the U. For Np:Np, the electron is removed from the NpO_3^- fragment to generate a NpO_3 fragment coupled to the NpO_3^+ fragment so that there is one spin on the Np +VI. Again, there are a number of close lying states for $Pu_2O_6^+$. The lowest energy structure has two Pu +VI with the electron removed from a bringing O to generate a sextet; note that unlike U:U, the electron is removed from one O to generate a lower symmetry structure

For **H**, the U:U structure is like bare $U_2O_6^+$, with two terminal ClO_4^- and with both U in the +VI state with the spin on the two bridging O atoms. For Np:Np, structure **H** corresponds to a

$Np_2O_6^+$ surrounded by two ClO_4^- in which the core $Np_2O_6^+$ contains one Np in the +VII oxidation state and Np +V with one unpaired spin. For Pu:Pu, the core structure looks like $Pu_2O_6^+$ with two +VI Pu and an electron removed from one bridging O to give sextet with low symmetry. The structure for Np:Pu follows that of $NpPuO_6^+$ with an Np in the +VII and the Pu in the +VI oxidation state. The results are consistent with the distinctive stability of heptavalent neptunium, as also established in condensed phase.[37-40] In addition, the results show that Pu does not really want to go beyond the +VI oxidation state.

Computed energies for perchlorate fission (**i**) and fragmentation (**ii**) are in Table 9 for native structures **A** and **D**, although from above, the latter is considered to be the actual structure. Based on previous studies, it is expected that the computed CID energies should be accessible under the employed moderate-energy conditions,[67] with the possible exception of 107.8 kcal/mol for fission pathway (**i**) for U:U structure **A**. For structure **D**, pathway (**i**) for all four complexes is computed as endothermic, with energies in a fairly narrow range of 41 to 55 kcal/mol, consistent with similar bonding for all An and constant An^V oxidation state in **D** and the fission products. In contrast to pathway (**i**), there is greater variation in the energy for pathway (**ii**) transformation of **D** to **H**, from substantially exothermic for U:U, to nearly thermoneutral for Np:Np and Np:Pu, and substantially endothermic for Pu:Pu (Table 9). Although rigorous assessment of CID kinetics would require computation of barriers on pathways (**i**) and (**ii**), the principles of Bell-Evans-Polanyi[68-69] and Hammond[70] suggest that transition state energies and resultant rates should generally correlate with net reaction energies as the reactions are significantly endothermic so the transition states will be very product-like. For all four actinide pairs**,** fission pathway (**i**) is higher energy than fragmentation (**ii**), with the differences ranging from substantial 91.3 kcal/mol for U:U to intermediate 45.3 kcal/mol for Np:Np and 41.3 kcal/mol for Np:Pu, to small 10.4 kcal/mol for Pu:Pu. In accord with the expected correspondence between kinetics and reaction energy, for the U:U complex low-energy pathway (**ii**) is entirely dominant over (**i**), whereas for the other three complexes the yields for the pathways are more similar (Figure 5). The observed abundance of pathway (**ii**) is significantly greater than for (**i**), except for the Pu:Pu complex where the two channels are comparable in accord with their similar computed energies. Such consistency between CID and theory bolsters confidence in the overall validity of the computations.

The CID results provide a further indication of relative stabilities of actinide oxidation states. Pathway (**ii**) entails oxidation of An^V in the native complex **D** to U^{VI}, Pu^{VI} or Np^{VII} (or intermediate $Np^{VI/VII}$) in **H**. The observed CID abundances, and computed energies and structures reveal that the ease of oxidation via pathway (**ii**) is highest for U^V to U^{VI} and lowest for Pu^V to Pu^{VI}. The intermediate pathway (**ii**) energy for Np^V corresponds to oxidation to Np^{VII} in Np:Pu or $Np^{VI/VII}$ in Np:Np. The results thus further demonstrate reduced stability of Pu^{VI} relative to Pu^V in an oxide coordination environment, and the distinctive stability of extreme oxidation state Np^{VII}.

Conclusions

Ion-molecule reactions and DFT calculations for gas-phase dinuclear complexes of uranium, neptunium and plutonium has revealed they contain actinides in oxidation states +V, +VI and +VII as actinyl moieties, which in some cases exhibit actinyl-actinyl interactions (AAIs). The

focus was on four native perchlorate complexes prepared by electrospray ionization (ESI), $[(AnO_2)_2(ClO_4)_3]^-$ having actinide pairs U:U, Np:Np, Pu:Pu and Np:Pu. DFT identified low-energy structure **D** consisting of actinyl(V) coordinated by perchlorates, $[(An^{V}O_2)_2(ClO_4)_3]^-$, and a higher-energy structure **A** containing a perchlorate ligand fragmented to ClO_3 and O, and actinyl(VI) (or plutonyl(V)): $[(An^{VI}O_2)(An^{V,VI}O_3)(ClO_4)_2(ClO_3)]^-$. Isomer **A** with oxidation state +VI is computed as lowest energy, except for the Pu:Pu complex. However, the observation that the U:U complex adsorbs O_2 suggests that it contains uranyl(V) available for oxidation, which excludes structure **A** and indicates instead **D** as the actual structure prepared by ESI. Structure **D** has all perchlorates intact, as expected for "soft" ESI. Addition of O_2 to **D** is computed as substantially exothermic only for the U:U complex, in accord with its observed reactivity. Structure **D** features an actinyl(V)-actinyl(V) interaction, $[(An^{V}O_2)\cdots(An^{V}O_2)(ClO_4)_3]^-$, which is disrupted by addition of O_2 as a peroxide bridge to yield actinyl(VI) complex, $[(An^{VI}O_2)(O_2)(An^{VI}O_2)(ClO_4)_3]^-$.

The computed energy difference between actinyl(V) isomer **D** and actinyl(VI) isomer **A** indicates oxidation from An^{V} to An^{VI} is most favorable for U, intermediate for Np, and least favorable for Pu. Similarly, conversion of actinyl(V) in isomer **D** to actinyl(VI) by addition of O_2 is exothermic for U, nearly thermoneutral for Np, and endothermic for Pu. For comparison, standard solution electrode potentials show that oxidation of $An^{V}O_2^{+}$ to $An^{VI}O_2^{2+}$ is most favorable for U, intermediate for Pu, and least favorable for Np. Whereas oxidation of +V to +VI is most facile for U^{V} in both solution and the gas-phase complexes, oxidation of Np^{V} is more favorable than Pu^{V} in the complexes whereas the reverse holds in solution. A key conclusion is thus that oxidation of An^{V} to An^{VI} by formation of actinide-oxygen bonds in the complexes—in contrast to oxidation by ionization and solvation—is more facile for Np versus Pu due to more effective Np-O bonding.

Collision induced dissociation of the native perchlorate complexes resulted in elimination of ClO_2 to yield $[(AnO_2)(O)_2(AnO_2)(ClO_4)_2]^-$. DFT computations indicate that the two extra O atoms in this product bridge the actinyls as oxo (O^{2-}) and/or oxyl (O^-) to yield oxidation states U^{VI}:U^{VI}, Pu^{VI}:Pu^{VI}, Np^{VII}:Pu^{VI}, and $Np^{VI/VII}$:$Np^{VI/VII}$ (VI/VII is intermediate state). The results reveal distinctive stability of heptavalent neptunium, formally neptunyl(VII) in $Np^{VII}O_2^{3+}$. The computed energy for the observed dissociation is lowest (substantially exothermic) for U:U and highest (substantially endothermic) for Pu:Pu, in accord with observed CID efficiencies of highest for U:U and lowest for Pu:Pu.

Supporting Information

ESI mass spectra of actinyl perchlorates. CID mass spectra for $[(UO_2)_2(NO_3)_3]^-$, $[(NpO_2)_2(NO_3)_3]^-$, $[(UO_2)_2Cl_3]^-$, $[(NpO_2)_2Cl_3]^-$ and $[(UO_2)(NpO_2)Cl_3]^-$. Reactivity results for $[(UO_2)_2(NO_3)_3]^-$ and $[(NpO_2)_2(NO_3)_3]^-$. Computed XYZ coordinates and IR frequencies; and overall spin multiplicities and selected Mulliken spin values.

Acknowledgements

This work was supported by the U. S. Department of Energy, Office of Science, Office of Basic Energy Sciences, Heavy Element Chemistry program at LBNL under Contract DE-AC02-05CH11231 (J.K.G., T.J.), and at The University of Alabama under Award DE-SC0018921 (D.A.D., M.V.). D.A.D. also thanks the Robert Ramsay Fund at The University of Alabama.

Table 1. Oxidation states, relative energies (ΔH_{0K} in kcal/mol) and spin multiplicities [in brackets] for native dimer structures **A**, **B**, **C** and **D** containing two actinides designated as An:An.[a]

Actinides	A	B	C	D
U:U	U^{VI}:U^{VI}/0.0 [1] [b] U^{V}:U^{V}/29.8 [3]	U^{VI}:U^{VI}/33.4 [3] U^{VI}:U^{VI}/45.5 [1]	U^{V}:U^{V}/81.2 [3]	U^{V}:U^{V}/53.2 [3]
Np:Np	Np^{VI}:Np^{VI}/0.0 [3] Np^{V}:Np^{VI}/9.3 [5]	Np^{VII}:Np^{VII} /11.8 [1] Np^{VI}:Np^{VII}/21.4 [3] Np^{VI}:Np^{VI}/30.9 [5]	Np^{V}:Np^{V}/31.4 [5]	Np^{V}:Np^{V}/20.8 [5]
Pu:Pu	Pu^{VI}:Pu^{V}/15.3 [5] Pu^{VI}:Pu^{V}/27.4 [7]	Pu^{VI}:Pu^{VI}/34.0 [3] Pu^{VI}:Pu^{VI}/38.0 [5] Pu^{VI}:Pu^{VI}/41.9 [7]	Pu^{V}:Pu^{V}/9.2 [7]	Pu^{V}:Pu^{V}/0.0 [7]
Np:Pu	Pu^{V}:Np^{VI}/0.0 [6][c] Pu^{VI}:Np^{VI}/0.5 [4][c] Np^{VI}:Pu^{V}/7.3 [4][d] Np^{VI}:Pu^{V}/12.7 [6][d]	Np^{VII}:$Pu^{V/VI}$/21.3 [2] Np^{VII}:Pu^{VI}/26.9 [4] Np^{VI}:Pu^{VI}/31.9 [6]	Np^{V}:Pu^{V}/25.8 [6]	Np^{V}:Pu^{V}/1.5 [6][e] Np^{V}:Pu^{V}/11.3 [6][f]

[a] Structure descriptions: **A** = $[(An^{VI}O_2^{2+})(An^{V,VI}O_3)(ClO_4^-)_2(ClO_3^-)]^-$; **B** = $[(An^{VI,VII}O_3^+)_2(ClO_4)_2(ClO_2)]^-$; **C** = $[(An^{V}O_2^+)_2(ClO_4^-)_3]^-$; **D** = $[(An^{V}O_2)_2(ClO_4)_3]^-$ (AAI). [b] There are two other singlet minima with different ClO_3^- coordination that are ~ 2.5 kcal/mol higher in energy. [c] AnO_2 An is Pu and AnO_3 An is Np. [d] AnO_2 An is Np and AnO_3 An is Pu. [e] Pu coordinated to two ClO_4^- and Np coordinated to 3 ClO_4^-. [f] Np coordinated to two ClO_4^- and Pu coordinated to 3 ClO_4^-.

Table 2. Selected distances (Å) and angles for native structures **A** and **D** shown in Figure 1.[a]

	A				D			
	U^{VI}:U^{VI}	Np^{VI}:Np^{VI}	Pu^{VI}:Pu^{V} [b]	Np^{VI}:Pu^{VI} [c]	U^{V}:U^{V}	Np^{V}:Np^{V}	Pu^{V}:Pu^{V}	Np^{V}:Pu^{V} [d]
a	1.76	1.74	1.72	1.73	1.79	1.77	1.76	1.77
a′	1.82	1.79	1.74	1.76	1.94	1.89	1.85	1.87
b	2.02	1.99	1.88	1.95	1.89	1.83	1.80	1.81
b′	1.81	1.79	1.77	1.79	1.81	1.77	1.76	1.76
b″	1.84	1.82	2.15	1.83	-	-	-	-
c	2.19	2.19	2.30	2.24	2.40	2.48	2.56	2.56
c′	2.57	2.59	2.92	2.74	2.26	2.31	2.36	2.33
α	178°	178°	178°	179°	174°	176°	176°	176°
β	162°	165°	180°	166°	173°	179°	179°	179°

[a] An-O_L distances (L = perchlorate) are 2.35-2.57 Å. **A** is lowest energy, except **D** for Pu:Pu.
[b] An*1* = Pu ($Pu^{VI}O_2^{2+}$); An*2* = Np ($Np^{VI}O_3$)
[c] An*1* = Pu^{VI} ($Pu^{VI}O_2^{2+}$); An*2* = Pu^{V} ($Pu^{V}O_3$)
[d] GS is An*1* = Np, An*2* = Pu; An*1* = Pu, An*2* = Np is 9.8 kcal/mol higher.

Table 3. Summary of observed ion-molecule reactions.[a]

Reactant Complex	O_2 addition?		H_2O addition?	
	Yes	No	Yes	No
$[(AnO_2)_2(ClO_4)_3]^-$	U:U[b]	Np:Np, Pu:Pu, Np:Pu	U:U[b], Np:Np	Pu:Pu, Np:Pu
$[(AnO_2)_2(NO_3)_3]^-$	U:U[b]	Np:Np	U:U[b]	Np:Np
$[(An^VO_2)_2Cl_3]^-$	U:U[b], U:Np	Np:Np	U:U[b], U:Np	Np:Np

[a] Yes = reaction observed; No = reaction not observed.

[b] Also sequential addition of O_2 and H_2O.

Table 4. Oxidation states and relative energies (ΔH_{0K} in kcal/mol) for products of O_2-addition.[a]

	O_2-adduct **$[(AnO_2)_2(O)_2(ClO_4)_3]^-$** [b]		
	E	**F**	**G**
U:U	U^{VI}:U^{V}/34.6 [1] U^{VI}:U^{V}/37.8 [3]	U^{VI}:U^{VI}/44.5 [3]	U^{VI}:U^{VI}/0.0 [1]
Np:Np	Np^{VI}:Np^{V}/28.1 [3] Np^{VI}:Np^{V}/30.5 [5] Np^{VI}:Np^{IV}/44.7 [7]	Np^{VI}:Np^{VI}/42.8 [5] Np^{VI}:Np^{VII}/32.7 [3] Np^{VII}:Np^{VII}/22.8 [1]	Np^{VI}:Np^{VI}/0.0 [3]
Pu:Pu	Pu^{V}:Pu^{IV}/39.3 [5] Pu^{V}:Pu^{IV}/43.1 [7] Pu^{V}:Pu^{V}/47.8 [9]	Pu^{VI}:Pu^{VI}/43.0 [3] Pu^{VI}:Pu^{VI}/47.1 [5] Pu^{VI}:Pu^{VI}/56.0 [7]	$Pu^{V/VI}$:$Pu^{V/VI}$/0.0[5]
Np:Pu	Np^{VI}:Pu^{IV}/26.6 [2] [c] Np^{VI}:Pu^{IV}/30.2 [4] [c] Np^{VI}:Pu^{IV}/30.0 [6] [c] Np^{VI}:Pu^{IV}/27.6 [8] [c] Pu^{VIII}:Np^{V}/51.5 [2] [d] Pu^{V}:Np^{V}/41.2 [4] [d] Pu^{V}:Np^{V}/43.6 [6] [d] Pu^{V}:Np^{V}/49.2 [8] [d]	[d]Np^{VII}:Pu^{VI}/47.3 [2] [d]Np^{VII}:Pu^{VI}/37.1 [4] [d]Np^{VI}:Pu^{VI}/34.5 [6] [e]Pu^{VI}:Np^{VII}/49.6 [2] [e]Pu^{VI}:Np^{VII}/37.0 [4] [e]Pu^{VI}:Np^{VI}/32.9 [6]	Np^{VI}:$Pu^{V/VI}$/0.0 [4]

[a] Spin multiplicities are in square brackets.

[b] Structure descriptions: **E** = $[(An^{VI}_2O_6^{2+})(ClO_4^-)_3]^-$,
F = $[(ClO_4^-)(An^{VI}O_3^+)(ClO_4^-)(An^{VI}O_3^+)(ClO_4^-)]^-$;
G = $[(ClO_4^-)(An^{VI}O_2^{2+})(ClO_4^-)(O_2^{2-})(An^{VI}O_2^{2+})(ClO_4^-)]^-$.

[c] An*1* = Np and An*2* = Pu. [d] An*1* = Pu and An*2* = Np.

Table 5. Selected distances (Å) and angles for structures **G** and **H**.[a]

	O_2-adduct **G** [b]				CID product **H**			
	U:U	Np:Np	Pu:Pu	Np:Pu	U^{VI}:U^{VI} [c]	$Np^{VI/VII}$:$Np^{VI/VII}$ [d]	Pu^{VI}:Pu^{VI}	Np^{VII}:Pu^{VI}
a	1.76	1.74	1.73	1.74	1.78	1.76	1.75	1.76
a′	1.76	1.74	1.73	1.74	1.78	1.76	1.75	1.76
b	1.76	1.74	1.73	1.73	1.78	1.76	1.74	1.74
b′	1.76	1.74	1.73	1.73	1.78	1.76	1.74	1.74
c	2.27	2.28	2.28	2.27	2.16	2.11	2.10	2.03
c′	2.41	2.40	2.40	2.41	2.16	2.11	2.35	2.03
d	2.27	2.28	2.28	2.28	2.16	2.11	2.11	2.21
d′	2.41	2.40	2.40	2.39	2.16	2.11	2.28	2.21
e	1.45	1.43	1.42	1.42	2.61	2.55	2.70	2.52
α	173°	175°	176°	176°	173°	172°	175°	169°
β	173°	175°	176°	176°	173°	172°	178°	177°

[a] Actinide pairs are An*1*:An*2* in Fig. 4. An-O_L distances (L = perchlorate) are 2.49-2.60 Å.
[b] Lowest-energy structure for the O_2-adduct; all actinide centers are An^{VI}.
[c] For the C_{2v} structure only 0.2 kcal/mol higher, ***c′*** = ***d*** but differ from ***c′*** = ***d′***.
[d] VI/VII designates oxidation state intermediate between +VI and +VII.

Table 6. Computed energies for O_2-addition to different structures of $[(AnO_2)_2(ClO_4)_3]^-$.[a]

	A→G	**B→G**	**C→G**	**D→G**
U:U	**18.8**	-14.6	-62.4	-34.4
Np:Np	**17.7**	5.9	-13.7	-3.1
Pu:Pu	4.5	-14.2	10.6	**19.8**
Np:Pu	**14.1**	-12.8	-11.7	12.7

[a] ΔH_{0K} in kcal/mol for O_2 addition to native complex structures **A** (lowest-energy for all except Pu/Pu), **B**, **C** and **D** (lowest-energy for Pu/Pu) to yield lowest-energy product **G**.

Table 7. Summary of CID results.

Precursor	**Pathway / products**	**Pathway observed?[b]**	
		Yes	**No**
$[(AnO_2)_2(ClO_4)_3]^-$	(**i**) $[(An^VO_2)(ClO_4)_2]^- + [(An^VO_2)(ClO_4)]$[a]	Np:Np, Pu:Pu Np:Pu	U:U
	(**ii**) $[(AnO_2)_2(O)_2(ClO_4)_2]^- + ClO_2$	U:U, Np:Np, Pu:Pu Np:Pu	
$[(AnO_2)_2(NO_3)_3]^-$	(**i**) $[(An^VO_2)(NO_3)_2]^- + [(An^VO_2)(NO_3)]$[a]	Np:Np	U:U
	(**iii**) $[(AnO_2)_2(O)_2(NO_3)_2]^- + NO$	U:U, Np:Np	
	(**iv**) $[(AnO_2)_2(O)_2(NO_3)]^- + 2NO_2$	U:U, Np:Np	
	(**v**) $[(AnO_2)_2(O)(NO_3)_2]^- + NO_2$	U:U	Np:Np
$[(An^VO_2)_2Cl_3]^-$	(**i**) $[(An^VO_2)Cl_2]^- + [(An^VO_2)Cl]$	U:U, Np:Np U:Np	

[a] Assigned oxidation state An(V) assumes intact perchlorates or nitrates.
[b] Yes = observed; No = not observed.

Table 8**.** Spin Multiplicities and Relative Energies (ΔH_{0K} in kcal/mol) for CID Product **H**. **$[(AnO_2)_2(O)_2(ClO_4)_2]^-$**.

Compound	Spin	Relative Energy
U^{VI}:U^{VI} (C_{2h})	2	0.0
Np^{VII}:Np^{VI} (C_s)	2	0.0
Np^{VII}:Np^{VI} (C_{2v})	2	3.2
Np^{VI}:Np^{VI} (C_s)	4	8.3
Np^{VI}:Np^{VI} (C_{2v})	2	11.8
Np^{VI}:Np^{VI} (C_{2v})	4	32.3
Pu^{VI}:Pu^{VI} (C_s)	6	0.0
Pu^{VI}:Pu^{VI} (C_s)	4	-2.2
Pu^{VII}:Pu^{VI} (C_{2v})	2	3.9
Pu^{VI}:Pu^{V} (C_{2v})[a]	6	20.9
Pu^{VI}:Pu^{V} (C_{2v})	8	18.0
Np^{VII}:Pu^{VI} (C_s)	3	0.0
Np^{VII}:Pu^{V} (C_s)	5	17.6
Np^{VI}:Pu^{VI} (C_s)	7	53.9

[a] Significant spin contamination.

Table 9. Computed energies (ΔH_{0K} in kcal/mol) of alternative dissociation pathways for $[(AnO_2)_2(ClO_4)_3]^-$.[a]

	Fission Pathway (**i**) to: $[(An^{V}O_2)(ClO_4)_2]^-$ + $[(An^{V}O_2)(ClO_4)]$		Fragmentation Pathway (**ii**) to: $[(AnO_2)_2(O)_2(ClO_4)_2]^-$ + ClO_2	
	A→products	**D→products**	**A→H**	**D→H**
U:U	107.8	54.6	16.5	-36.7
Np:Np	62.9	42.1	5.8	-15.0
Pu:Pu	25.7	41.0	9.2	24.5
Np:Pu	47.4[a]	46.0[a]	6.2	4.7

[a] Average for channels producing anions $[(Np^{V}O_2)(ClO_4)_2]^-$ and $[(Pu^{V}O_2)(ClO_4)_2]^-$; the latter pathway is 0.4 kcal/mol higher energy.

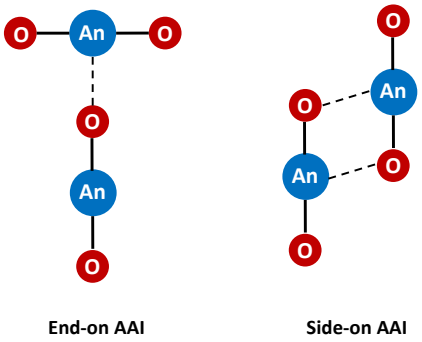

Scheme 1. Two types of actinyl-actinyl interaction (AAI; also referred to as “cation-cation interaction”): Left, end-on T-shaped; Right, side-on diamond shaped.

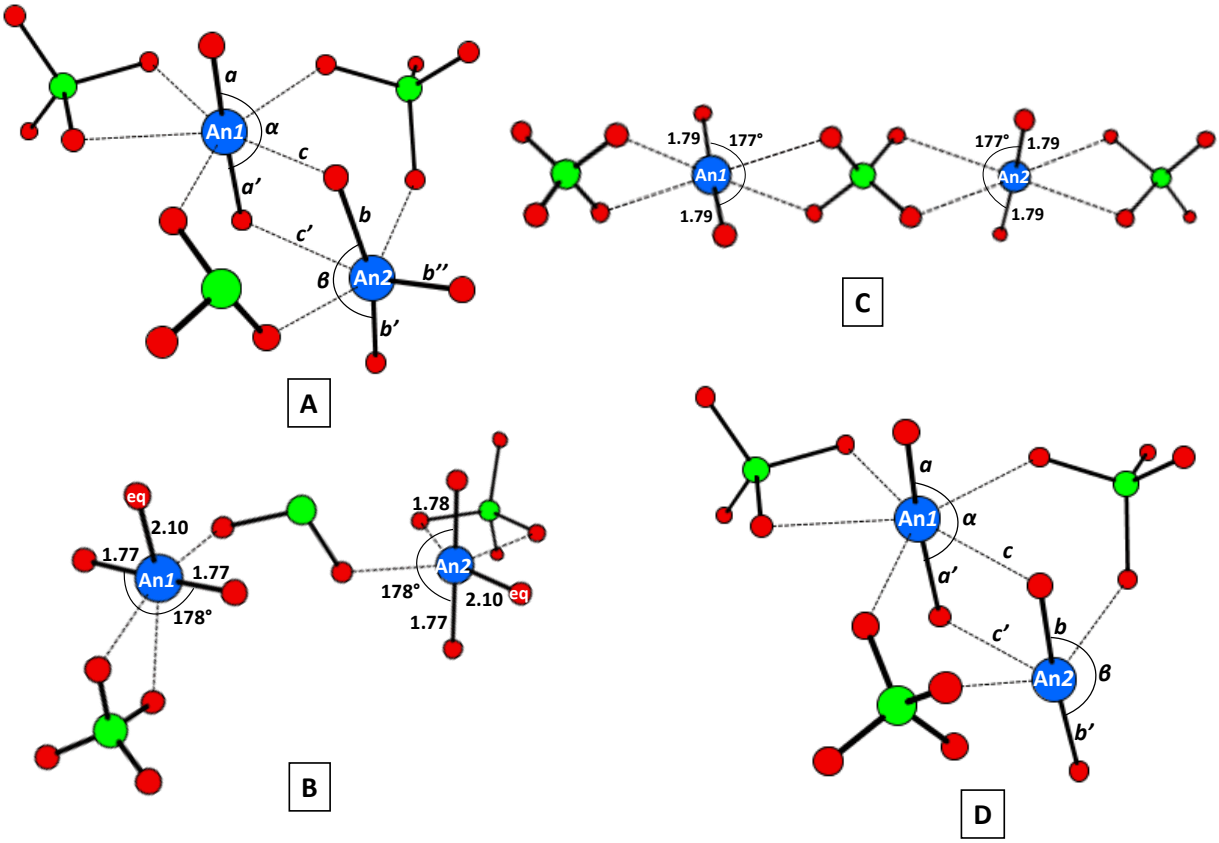

Figure 1. Computed structures **A**, **B**, **C** and **D** for native dimers $[(AnO_2)_2(ClO_4)_3]^-$; in **A** and **B** a perchlorate is fragmented. Blue balls = actinides An*1* and An*2*; red = O; green = Cl. Selected distances (Å) and angles for An*1*:An*2* = U:U are given for **B** and **C**; values for labelled bonds and angles in **A** and **D** are in Table 2. Covalent and dative bonds are respectively solid and dotted lines (bond ***c*** in **A** is intermediate).

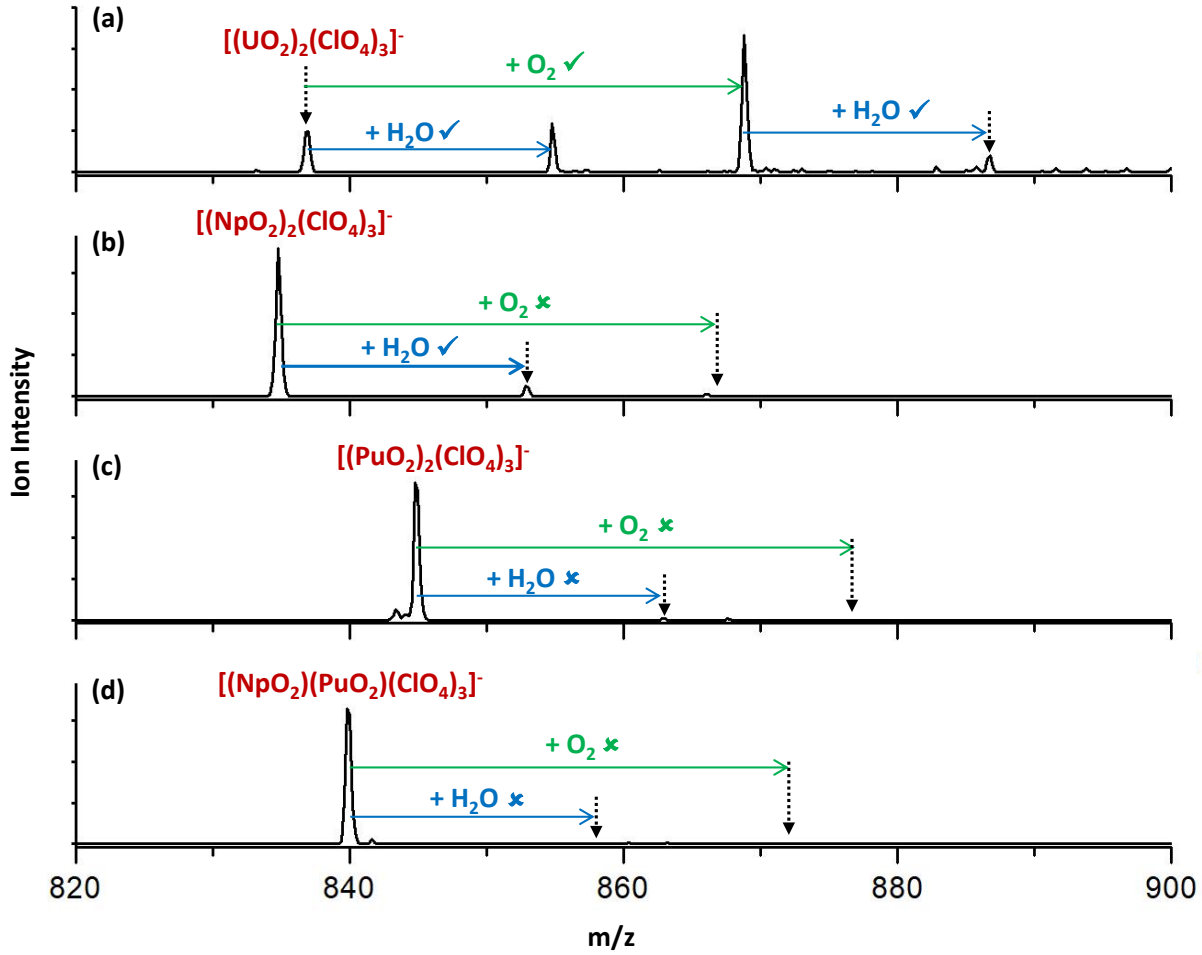

Figure 2. Mass spectra obtained after isolation of (a) $[(UO_2)_2(ClO_4)_3]^-$ for 10 s; (b) $[(NpO_2)_2(ClO_4)_3]^-$ for 10 s; (c) $[(PuO_2)_2(ClO_4)_3]^-$ for 0.8 s; (d) $[(NpO_2)(PuO_2)(ClO_4)_3]^-$ for 0.8 s. Addition reactions with background O_2 and H_2O are indicated as ✓ = reaction, and ✗ = no reaction. Maximum ion intensities on the y-axis are: (a) 300, (b) 50000, (c) 800 and (d) 700.

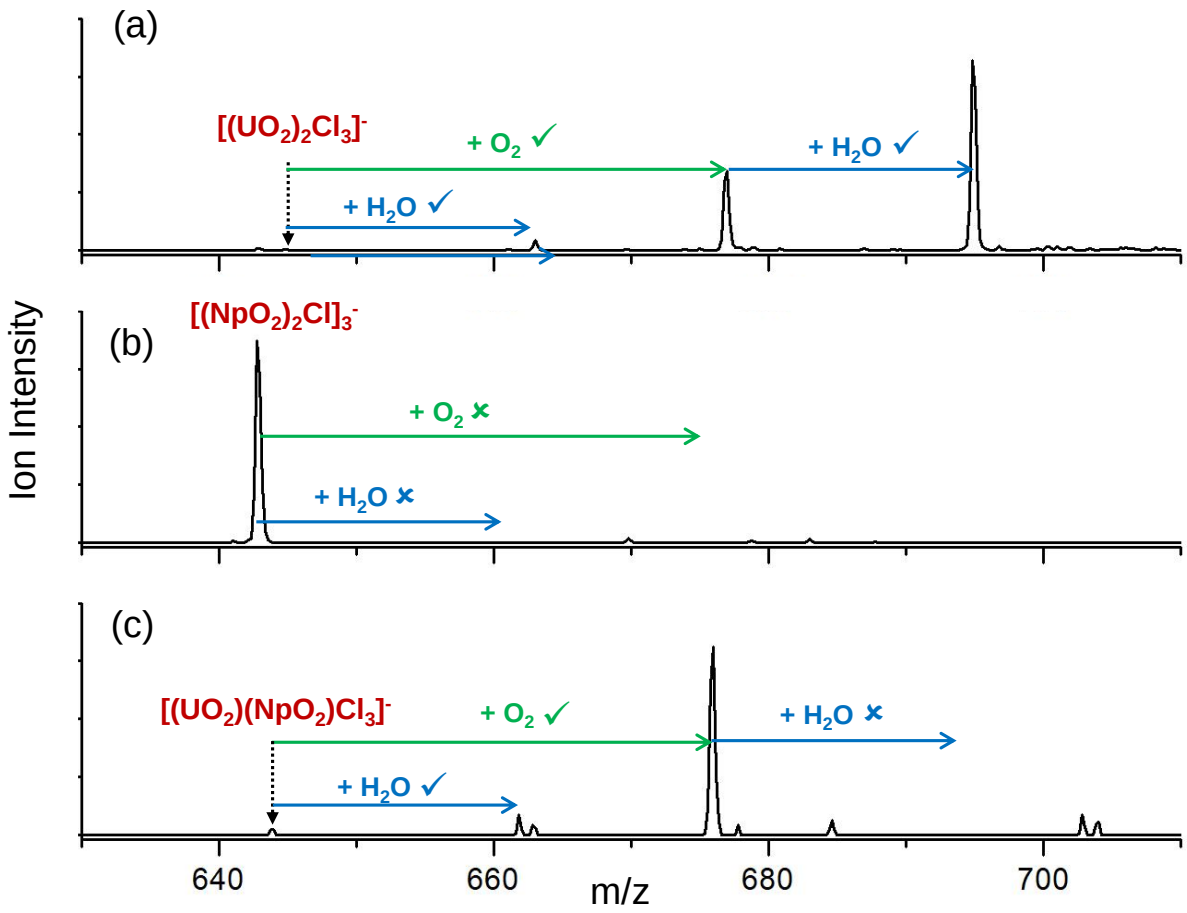

Figure 3. Mass spectra obtained after 10 s isolation for (a) $[(UO_2)_2Cl_3]^-$; (b) $[(NpO_2)_2Cl_3]^-$; (c) $[(UO_2)(NpO_2)Cl_3]^-$. Reactions with background gases O_2 and H_2O are indicated (✓ = reaction; × = no reaction). Maximum ion intensities on the y-axis are: (a) 3400, (b) 44000 and (c) 240.

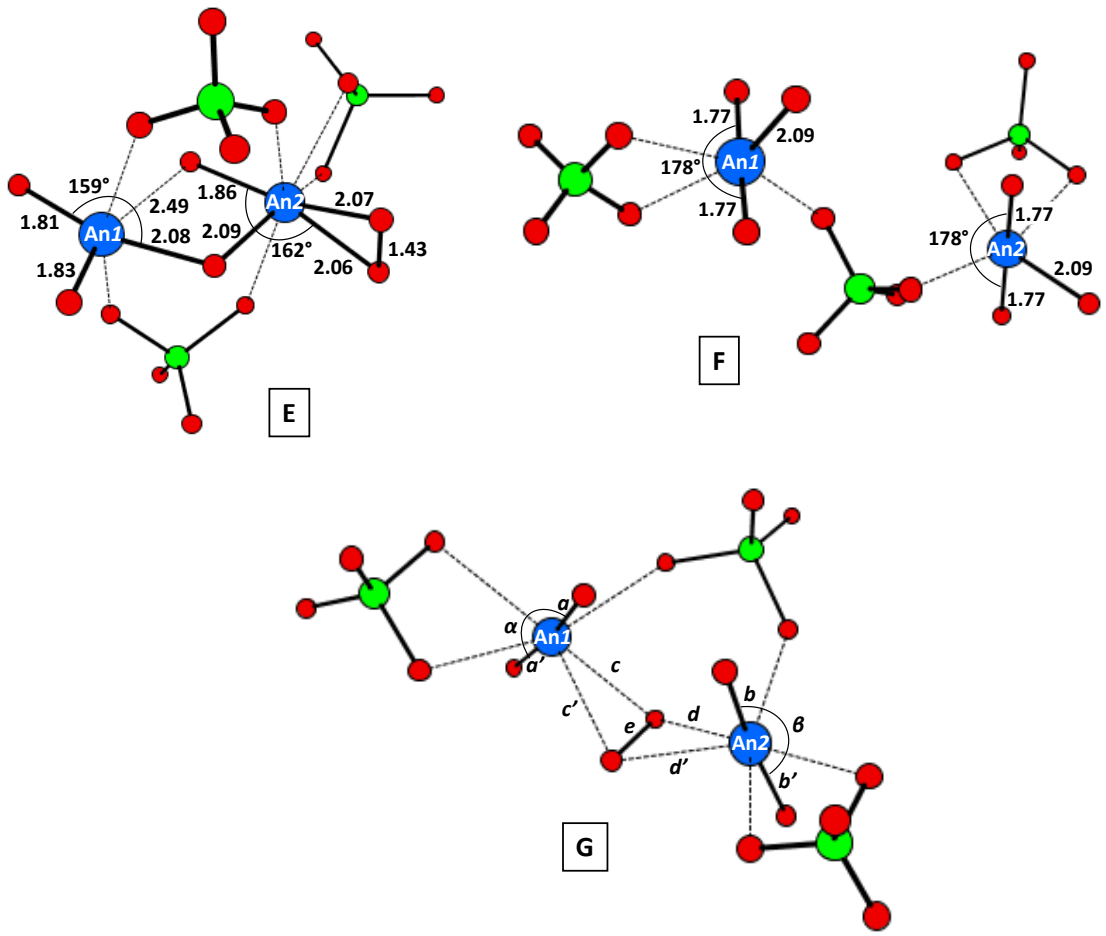

Figure 4. Computed structures **E**, **F** and **G** for O_2-adducts to the native dimers. Blue balls = actinides An*1* and An*2*; red = O; green = Cl. Selected distances (Å) and angles for An*1*:An*2* = U:U are given for **E** and **F**; values for labelled bonds and angles in **G** are in Table 5. Covalent and dative bonds are respectively solid and dotted lines. The long distance of 2.52 Å between bridging O atoms in **E** indicates negligible O-O bonding.

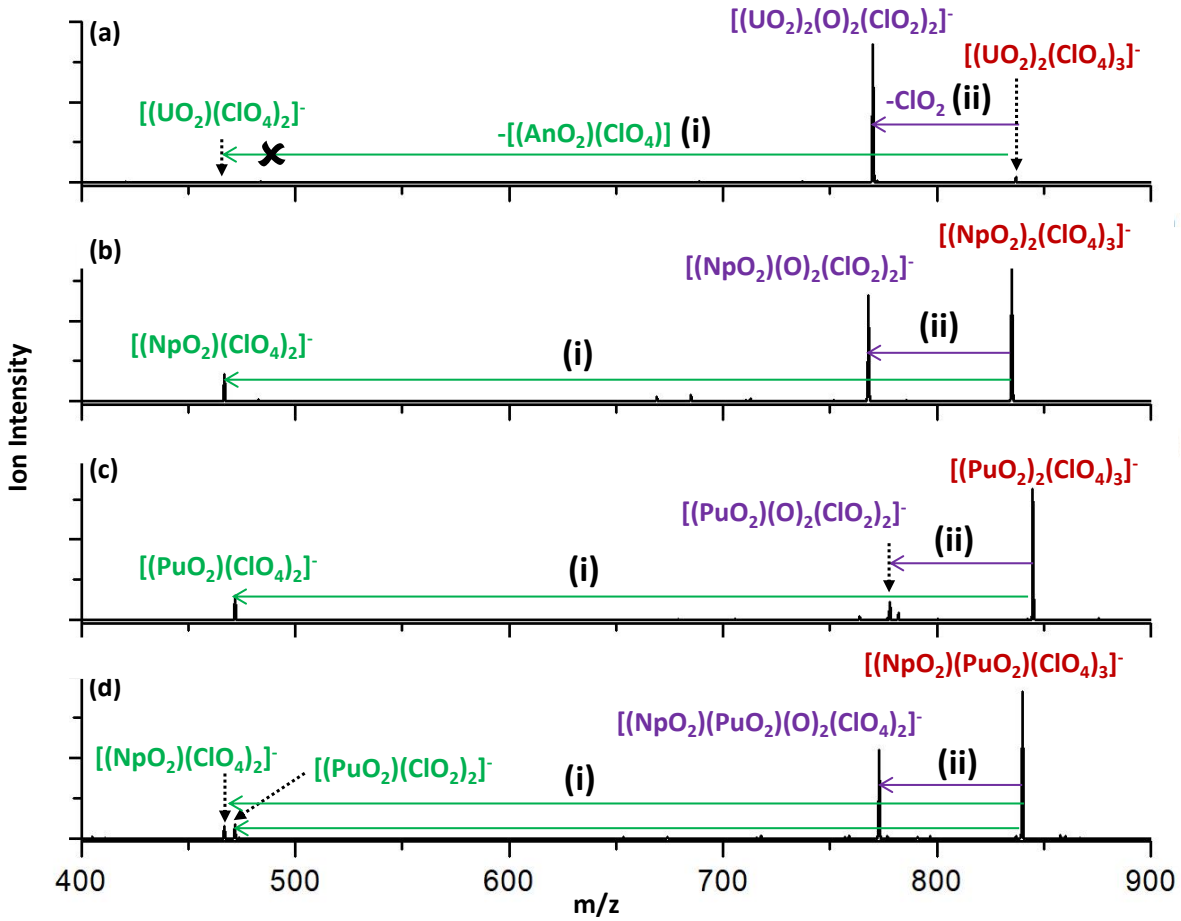

Figure 5. CID mass spectra for (a) $[(UO_2)_2(ClO_4)_3]^-$; (b) $[(NpO_2)_2(ClO_4)_3]^-$; (c) $[(PuO_2)_2(ClO_4)_3]^-$; (d) $[(NpO_2)(PuO_2)(ClO_4)_3]^-$ with the dissociation channels (**i**) and (**ii**) as given in Table 8. Nominal applied CID voltage is 0.40 V. The maximum ion intensities on the y-axis are: (a) 1400, (b) 30000, (c) 700 and (d) 600.

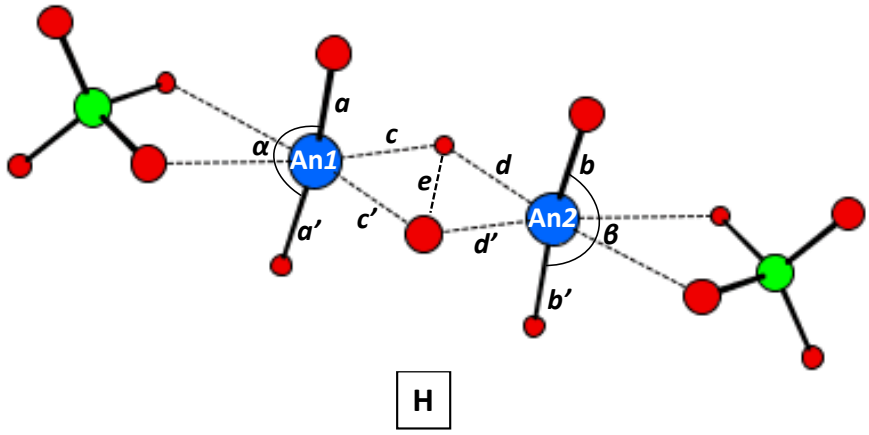

Figure 6. Computed structure **H** for CID products. Blue balls = actinides An*1* and An*2*; red = O; green = Cl. Labelled distances (Å) and angles are in Table 5. Distance ***e*** is long, indicating negligible O-O bonding. The oxidation state assignments for the four CID products are U^{VI}:U^{VI}, $Np^{VI/VII}$:$Np^{VI/VII}$ (intermediate state), Pu^{VI}:Pu^{VI} and Np^{VII}:Pu^{VI}.

References

1. Li, G. F.; Zhu, D. X.; Wang, X. L.; Su, Z. M.; Bryce, M. R., Dinuclear Metal Complexes: Multifunctional Properties and Applications. *Chem Soc Rev* **2020,** *49*, 765-838.
2. Mougel, V.; Horeglad, P.; Nocton, G.; Pecaut, J.; Mazzanti, M., Stable Pentavalent Uranyl Species and Selective Assembly of a Polymetallic Mixed-Valent Uranyl Complex by Cation-Cation Interactions. *Angew Chem Int Edit* **2009,** *48*, 8477-8480.
3. Choppin, G. R.; Rao, L. F., Complexation of Pentavalent and Hexavalent Actinides by Fluoride. *Radiochim Acta* **1984,** *37*, 143-146.
4. Lucena, A. F.; Carretas, J. M.; Marçalo, J.; Michelini, M. D.; Rutkowski, P. X.; Gibson, J. K., Dissociation of Gas-Phase Bimetallic Clusters as a Probe of Charge Densities: The Effective Charge of Uranyl. *J Phys Chem A* **2014,** *118*, 2159-2166.
5. Gilson, S. E.; Fairley, M.; Hanna, S. L.; Szymanowski, J. E. S.; Julien, P.; Chen, Z. J.; Farha, O. K.; LaVerne, J. A.; Burns, P. C., Unusual Metal-Organic Framework Topology and Radiation Resistance through Neptunyl Coordination Chemistry. *J Am Chem Soc* **2021,** *143*, 17354-17359.
6. Pyrch, M. M.; Augustine, L. J.; Williams, J. M.; Mason, S. E.; Forbes, T. Z., Use of Vibrational Spectroscopy to Identify the Formation of Neptunyl-Neptunyl Interactions: A Paired Density Functional Theory and Raman Spectroscopy Study. *Dalton T* **2022,** *51*, 4772-4785.
7. Cousson, A.; Dabos, S.; Abazli, H.; Nectoux, F.; Pages, M.; Choppin, G., Crystal-Structure of a Neptunyl Cation-Cation Complex (NpO_2^+) with Mellitic Acid - $Na_4(NpO_2)_2C_{12}O_{12}.8H_2O$. *J Less-Common Met* **1984,** *99*, 233-240.
8. Albrecht-Schmitt, T. E.; Almond, P. M.; Sykora, R. E., Cation-Cation Interactions in Neptunyl(V) Compounds: Hydrothermal Preparation and Structural Characterization of $NpO_2(IO_3)$ and alpha- and beta-$AgNpO_2(SeO_3)$. *Inorg Chem* **2003,** *42*, 3788-3795.
9. Sullens, T. A.; Jensen, R. A.; Shvareva, T. Y.; Albrecht-Schmitt, T. E., Cation-Cation Interactions Between Uranyl Cations in a Polar Open-Framework Uranyl Periodate. *J Am Chem Soc* **2004,** *126*, 2676-2677.
10. Feng, R. L.; Glendening, E. D.; Peterson, K. A., Actinyl Cation-Cation Interactions in the Gas Phase: an Accurate Thermochemical Study. *Phys Chem Chem Phys* **2019,** *21*, 7953-7964.
11. Hu, S. X.; Jian, J. W.; Li, J.; Gibson, J. K., Destruction of the Uranyl Moiety in a U(V) "Cation-Cation" Interaction. *Inorg Chem* **2019,** *58*, 10148-10159.
12. Maurice, R.; Dau, P. D.; Hodee, M.; Renault, E.; Gibson, J. K., Controlling Cation-Cation Interactions in Uranyl Coordination Dimers by Varying the Length of the Dicarboxylate Linker. *Eur J Inorg Chem* **2020,** *2020*, 4465-4476.
13. Naiini, A. A.; Pinkas, J.; Plass, W.; Young, V. G.; Verkade, J. G., Triethanolamine Complexes of H^+, Li^+, Na^+, Sr^{2+}, and Ba^{2+} Perchlorates. *Inorg Chem* **1994,** *33*, 2137-2141.
14. Urabe, T.; Tsugoshi, T.; Tanaka, M., Electrospray Ionization Mass Spectrometry Investigation of the Blocking Effect of Sulfate on the Formation of Aluminum Tridecamer. *J Mol Liq* **2008,** *143*, 70-74.
15. House, D. A.; Steel, P. J.; Watson, A. A., Chiral Heterocyclic-Compounds .5. The 1st X-Ray Structure of an Octahedral Transition-Metal Complex Containing a Strongly Chelating Bidentate Perchlorate. *J Chem Soc Chem Comm* **1987**, 1575-1576.
16. Pascal, J. L.; Potier, J.; Jones, D. J.; Roziere, J.; Michalowicz, A., Structural Approach to the Behavior of ClO_4^- as a Ligand in Transition-Metal Complexes Using EXAFS, Ir, and Raman-Spectroscopy .1. A Perchlorate-Bridged Copper Chain with Short Copper Copper Distances in $Cu(ClO_4)_2$. *Inorg Chem* **1984,** *23*, 2068-2073.
17. Komaei, S. A.; van Albada, G. A.; Haasnoot, J. G.; Kooijman, H.; Spek, A. L.; Reedijk, J., Synthesis, Spectroscopic, Magnetic Properties and X-Ray Crystal Structure of Di-Mu-Hydroxo-Bis(Mu-Perchlorato-

O,O')Bis-[Bis(2-Amino-4-Methylpyrimidine)Copper(II)]: Bridging Perchlorate Results in Significant Deviation from the Predicted Magnetic Exchange. *Inorg Chim Acta* **1999,** *286*, 24-29.
18. Sinha, R. K.; Nicol, E.; Steinmetz, V.; Maitre, P., Gas Phase Structure of Micro-Hydrated $[Mn(ClO_4)]^+$ and $[Mn_2(ClO_4)_3]^+$ Ions Probed by Infrared Spectroscopy. *J Am Soc Mass Spectr* **2010,** *21*, 758-772.
19. Sessler, J. L.; Seidel, D.; Vivian, A. E.; Lynch, V.; Scott, B. L.; Keogh, D. W., Hexaphyrin(1.0.1.0.0.0): An Expanded Porphyrin Ligand for the Actinide Cations Uranyl (UO_2^{2+}) and Neptunyl (NpO_2^+). *Angew Chem Int Edit* **2001,** *40*, 591-594.
20. Bagnall, K. W.; Laidler, J. B.; Stewart, M. A. A., Americyl(V) and Americyl(VI) Chloro-Complexes. *Chem Commun* **1967**, 24-25.
21. Burn, A. G.; Nash, K. L., Electrochemical Behavior of Uranyl in Anhydrous Polar Organic Media. *Radiochim Acta* **2017,** *105*, 513-522.
22. Dau, P. D.; Dau, P. V.; Rao, L. F.; Kovács, A.; Gibson, J. K., A Uranyl Peroxide Dimer in the Gas Phase. *Inorg Chem* **2017,** *56*, 4186-4196.
23. Rios, D.; Michelini, M. C.; Lucena, A. F.; Marçalo, J.; Bray, T. H.; Gibson, J. K., Gas-Phase Uranyl, Neptunyl, and Plutonyl: Hydration and Oxidation Studied by Experiment and Theory. *Inorg Chem* **2012,** *51*, 6603-6614.
24. Rios, D.; Rutkowski, P. X.; Shuh, D. K.; Bray, T. H.; Gibson, J. K.; Van Stipdonk, M. J., Electron Transfer Dissociation of Dipositive Uranyl and Plutonyl Coordination Complexes. *J Mass Spectrom* **2011,** *46*, 1247-1254.
25. Becke, A. D., Density-Functional Thermochemistry .3. The Role of Exact Exchange. *J Chem Phys* **1993,** *98*, 5648-5652.
26. Lee, C. T.; Yang, W. T.; Parr, R. G., Development of the Colle-Salvetti Correlation-Energy Formula into a Functional of the Electron-Density. *Phys Rev B* **1988,** *37*, 785-789.
27. Kendall, R. A.; Dunning, T. H.; Harrison, R. J., Electron-Affinities of the 1st-Row Atoms Revisited - Systematic Basis-Sets and Wave-Functions. *J Chem Phys* **1992,** *96*, 6796-6806.
28. Dunning, T. H.; Peterson, K. A.; Wilson, A. K., Gaussian Basis Sets for use in Correlated Molecular Calculations. X. The Atoms Aluminum Through Argon Revisited. *J Chem Phys* **2001,** *114*, 9244-9253.
29. Küchle, W.; Dolg, M.; Stoll, H.; Preuss, H., Energy-Adjusted Pseudopotentials for the Actinides - Parameter Sets and Test Calculations for Thorium and Thorium Monoxide. *J Chem Phys* **1994,** *100*, 7535-7542.
30. Cao, X.; Dolg, M., Segmented contraction scheme for small-core actinide pseudopotential basis sets. *J. Mol. Struct. (Theochem)* **2004,** *673*, 203-209.
31. Cao, X. Y.; Dolg, M.; Stoll, H., Valence Basis Sets for Relativistic Energy-Consistent Small-Core Actinide Pseudopotentials. *J Chem Phys* **2003,** *118*, 487-496.
32. Frisch, M. J.; Trucks, G. W.; Schlegel, H. B.; Scuseria, G. E.; Robb, M. A.; Cheeseman, J. R.; Scalmani, G.; Barone, V.; Petersson, G. A.; Nakatsuji, H., et al. *Gaussian 16, Revision A.03*, Wallingford, CT, 2016.
33. Bratsch, S. G., Standard Electrode-Potentials and Temperature Coefficients in Water at 298.15 K. *J Phys Chem Ref Data* **1989,** *18*, 1-21.
34. Blair, S. M.; Brodbelt, J. S.; Reddy, G. M.; Marchand, A. P., Evaluation of Binding Selectivities of Bis-Crowned Clefts by Electrospray Ionization Quadrupole Ion Trap Mass Spectrometry. *J Mass Spectrom* **1998,** *33*, 721-728.
35. Anbalagan, V.; Chien, W.; Gresham, G. L.; Groenewold, G. S.; Van Stipdonk, M. J., Production and Collision-Induced Dissociation of Gas-Phase, Water- and Alcohol-Coordinated Uranyl Complexes Containing Halide or Perchlorate Anions. *Rapid Commun Mass Sp* **2004,** *18*, 3028-3034.

36. Sokalska, M.; Prussakowska, M.; Hoffmann, M.; Gierczyk, B.; Franski, R., Unusual Ion UO_4^- Formed Upon Collision Induced Dissociation of $[UO_2(NO_3)_3]^-$, $[UO_2(ClO_4)_3]^-$, $[UO_2(CH_3COO)_3]^-$ Ions. *J Am Soc Mass Spectr* **2010,** *21*, 1789-1794.
37. Spitsyn, V. I.; Krot, N. N.; Mefodeva, M. P.; Gelman, A. D., Methods of Heptavalent Neptunium Production. *Dokl Akad Nauk SSSR* **1968,** *181*, 128-130.
38. Spitsyn, V. I.; Gelman, A. D.; Krot, N. N.; Mefodiye.Mp; Zakharov.Fa; Komkov, Y. A.; Shilov, V. P.; Smirnova, I. V., Heptavalent State of Neptunium and Plutonium. *J Inorg Nucl Chem* **1969,** *31*, 2733-2745.
39. Tananaev, I. G.; Nikonov, M. V.; Myasoedov, B. F.; Clark, D. L., Plutonium in Higher Oxidation States in Alkaline Media. *J Alloy Compd* **2007,** *444*, 668-672.
40. Krot, N. N.; Charushnikova, I. A., Synthesis, Structure, and Properties of Actinide(VII) Compounds. *Radiochemistry* **2021,** *63*, 683-716.
41. Nocton, G.; Horeglad, P.; Pecaut, J.; Mazzanti, M., Polynuclear Cation-Cation Complexes of Pentavalent Uranyl: Relating Stability and Magnetic Properties to Structure. *J Am Chem Soc* **2008,** *130*, 16633-16645.
42. Vasiliu, M.; Gibson, J. K.; Peterson, K. A.; Dixon, D. A., Gas Phase Hydrolysis and Oxo-Exchange of Actinide Dioxide Cations: Elucidating Intrinsic Chemistry from Protactinium to Einsteinium. *Chem-Eur J* **2019,** *25*, 4245-4254.
43. Gabelnick, S. D.; Reedy, G. T.; Chasanov, M. G., Infrared-Spectrum of Matrix-Isolated Uranium Oxide Vapor Species. *Chem Phys Lett* **1973,** *19*, 90-93.
44. Ronchi, C.; Capone, F.; Colle, J. Y.; Hiernaut, J. P., Volatile Molecule PuO_3 Observed from Subliming Plutonium Dioxide. *J Nucl Mater* **2000,** *280*, 111-115.
45. Gabelnick, S. D.; Reedy, G. T.; Chasanov, M. G., Infrared-Spectra of Matrix-Isolated Uranium Oxide Species. II. Spectral Interpretation and Structure of UO_3. *J Chem Phys* **1973,** *59*, 6397-6404.
46. Hunt, R. D.; Andrews, L., Reactions of Pulsed-Laser Evaporated Uranium Atoms with Molecular-Oxygen - Infrared-Spectra of UO, UO_2, UO_3, UO_2^+, UO_2^{2+}, and UO_3-O_2 in Solid Argon. *J Chem Phys* **1993,** *98*, 3690-3696.
47. Konings, R. J. M.; Benes, O.; Kovács, A.; Manara, D.; Sedmidubsky, D.; Gorokhov, L.; Iorish, V. S.; Yungman, V.; Shenyavskaya, E.; Osina, E., The Thermodynamic Properties of the f- Elements and their Compounds. Part 2. The Lanthanide and Actinide Oxides. *J Phys Chem Ref Data* **2014,** *43*.
48. Marçalo, J.; Gibson, J. K., Gas-Phase Energetics of Actinide Oxides: An Assessment of Neutral and Cationic Monoxides and Dioxides from Thorium to Curium. *J Phys Chem A* **2009,** *113*, 12599-12606.
49. Kovács, A., Molecular Oxides of High-Valent Actinides. *Struct Chem* **2020,** *31*, 1247-1271.
50. Kovács, A., Relativistic Multireference Quantum Chemical Study of the Electronic Structure of Actinide Trioxide Molecules. *J Phys Chem A* **2017,** *121*, 2523-2530.
51. Zaitsevskii, A., Plutonium and Transplutonium Element Trioxides: Molecular Structures, Chemical Bonding, and Isomers. *Phys Chem Chem Phys* **2015,** *17*, 24831-24836.
52. Denning, R. G., Electronic Structure and Bonding in Actinyl Ions and their Analogs. *J Phys Chem A* **2007,** *111*, 4125-4143.
53. Lennard-Jones, J. E., Processes of Adsorption and Diffusion on Solid Surfaces. *T Faraday Soc* **1932,** *28*, 0333-0358.
54. Langmuir, I., Forces Near the Surfaces of Molecules. *Chem Rev* **1929,** *6*, 451-479.
55. Stockigt, D.; Schwarz, H., Distinction of Fe^+-NCH and Fe^+-CNH Complexes by Gas-Phase Ion-Molecule Reactions. *Chem Ber* **1994,** *127*, 791-793.
56. Lias, S. G.; Bartmess, J. E.; Liebman, J. F.; Holmes, J. L.; Levin, R. D.; Mallard, W. G., Gas-Phase Ion and Neutral Thermochemistry. *J Phys Chem Ref Data* **1988,** *17*, 1-861.
57. Ricks, A. M.; Gagliardi, L.; Duncan, M. A., Uranium Oxo and Superoxo Cations Revealed Using Infrared Spectroscopy in the Gas Phase. *J Phys Chem Lett* **2011,** *2*, 1662-1666.

58. Molina-Svendsen, H.; Bojesen, G.; McKenzie, C. J., Gas-Phase Reactivity of Coordinatively Unsaturated Transition Metal Complex Ions Toward Molecular Oxygen. *Inorg Chem* **1998,** *37*, 1981-1983.
59. Fiedler, A.; Kretzschmar, I.; Schröder, D.; Schwarz, H., Chromium Dioxide Cation $OCrO^+$ in the Gas Phase: Structure, Electronic States, and the Reactivity with Hydrogen and Hydrocarbons. *J Am Chem Soc* **1996,** *118*, 9941-9952.
60. Koyanagi, G. K.; Caraiman, D.; Blagojevic, V.; Böhme, D. K., Gas-Phase Reactions of Transition-Metal Ions with Molecular Oxygen: Room-Temperature Kinetics and Periodicities in Reactivity. *J Phys Chem A* **2002,** *106*, 4581-4590.
61. Tang, W. K.; Chau, M. C.; Siu, C. K., Role of Water in Molecular Oxygen Activation in Hydrated Chromium(I) Cluster Ions: A Theoretical Insight. *Int J Mass Spectrom* **2019,** *436*, 118-126.
62. Gong, Y.; Gibson, J. K., Formation and Characterization of the Uranyl-SO_2 Complex, $UO_2(CH_3SO_2)(SO_2)^-$. *J Phys Chem A* **2013,** *117*, 783-787.
63. Lucena, A. F.; Carretas, J. M.; Marçalo, J.; Michelini, M. C.; Gong, Y.; Gibson, J. K., Gas-Phase Reactions of Molecular Oxygen with Uranyl(V) Anionic Complexes-Synthesis and Characterization of New Superoxides of Uranyl(VI). *J Phys Chem A* **2015,** *119*, 3628-3635.
64. Vallet, V.; Wahlgren, U.; Schimmelpfennig, B.; Moll, H.; Szabo, Z.; Grenthe, I., Solvent Effects on Uranium(VI) Fluoride and Hydroxide Complexes Studied by EXAFS and Quantum Chemistry. *Inorg Chem* **2001,** *40*, 3516-3525.
65. Renault, E.; Jian, J. W.; Maurice, R.; van Stipdonk, M. J.; Tatosian, I. J.; Bubas, A. R.; Martens, J.; Berden, G.; Oomens, J.; Gibson, J. K., Characterization of Uranyl Coordinated by Equatorial Oxygen: Oxo in UO_3 versus Oxyl in UO_3^+. *J Phys Chem A* **2021,** *125*, 5544-5555.
66. Cramer, C. J.; Tolman, W. B.; Theopold, K. H.; Rheingold, A. L., Variable Character of O-O and M-O Bonding in Side-On (eta(2)) 1 : 1 Metal Complexes of O-2. *P Natl Acad Sci USA* **2003,** *100*, 3635-3640.
67. Gong, Y.; de Jong, W. A.; Gibson, J. K., Gas Phase Uranyl Activation: Formation of a Uranium Nitrosyl Complex from Uranyl Azide. *J Am Chem Soc* **2015,** *137*, 5911-5915.
68. Bell, R. P., The Mechanism of the N-Halogenoacylanilide Rearrangements. *J Chem Soc* **1936**, 1154-1156.
69. Evans, M. G.; Polanyi, M., Further Considerations on the Thermodynamics of Chemical Equilibria and Reaction Rates. *T Faraday Soc* **1936,** *32*, 1333-1359.
70. Hammond, G. S., A Correlation of Reaction Rates. *J Am Chem Soc* **1955,** *77*, 334-338.

TOC Graphic

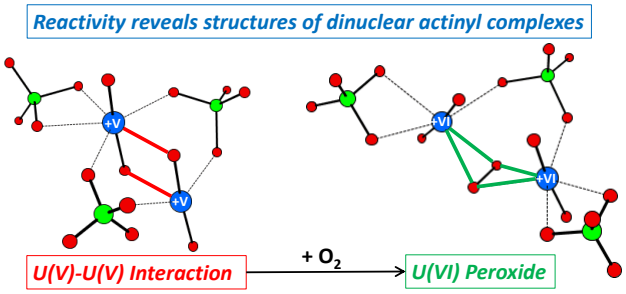
Reactivity reveals structures of dinuclear actinyl complexes
+V
+V
+VI
+VI
U(V)-U(V) Interaction
+ O2
U(VI) Peroxide